

Function of mTOR complex 1 and 2 in Skeletal Muscle

Inauguraldissertation

zur
Erlangung der Würde eines Doktors der Philosophie
vorgelegt der
Philosophisch-Naturwissenschaftlichen Fakultät
der Universität Basel
von

Conrad Florian Bentzinger

aus Basel (BS)

Biozentrum der Universität Basel
Basel, 2009



Genehmigt von der Philosophisch-Naturwissenschaftlichen Fakultät auf Antrag von:

Prof. Dr. Markus A. Rüegg
Dissertationsleitung

PD Dr. Francesco Zorzato
Korreferat

Basel, den 13. Januar 2009

Prof. Dr. Eberhard Parlow
Dekan der Philosophisch-Naturwissenschaftlichen Fakultät

“Obsessed is just a word the lazy use to describe the dedicated.”

Russell Warren

TABLE OF CONTENTS

1. SUMMARY	5
1.1 List of abbreviations	6
2. INTRODUCTION	8
2.1. Catching a glimpse of mTOR and its role in skeletal muscle.....	8
2.1.1. mTOR mediated muscle growth	8
2.1.2. Nutrients and mTOR.....	9
2.1.3. mTOR balances cellular energy generation	10
2.1.4. mTOR regulated autophagy	10
2.1.5. Bottom line on the role of mTOR in skeletal muscle.....	10
2.2. The PKB/AKT and mTOR signaling pathway	12
2.3. mTOR complex 1 and 2	14
2.4. Protein kinase B / AKT	16
2.5. The tuberous sclerosis complex	18
2.6. Downstream targets of mTORC1.....	20
2.7. Downstream targets of mTORC2.....	21
2.8. The negative feedback from S6K.....	21
3. RESULTS	22
3.1. Skeletal muscle-specific ablation of raptor and rictor	22
3.2. Deficiency of mTORC1 but not mTORC2 causes muscle dystrophy	23
3.3. Skeletal muscles of RAmKO mice show alterations in their metabolic and structural properties	24
3.4. Functional characterization of muscles in RAmKO mice	25
3.5. Inactivation of raptor or rictor affects activation of PKB/AKT	25
3.6. Genes involved in mitochondrial biogenesis are downregulated in RAmKO mice	26
3.7. Activation of PKB/AKT is independent of mTORC2	27
4. DISCUSSION	28
4.1. Raptor is required for high oxidative capacity of skeletal muscle	28
4.2. Segregation of metabolic and structural properties in skeletal muscle of RAmKO mice.....	29
4.3. Raptor deficiency affects protein synthesis directly and PKB/AKT activation indirectly	29
4.4. Raptor-deficient skeletal muscles are small, despite high energy consumption	30
4.5. Hyperactivation of PKB/AKT does not require rictor/mTORC2.....	30
5. EXPERIMENTAL PROCEDURES	32
6. TABLES	36
7. FIGURES AND FIGURE LEGENDS	37
Figure 1. Targeting strategy and initial characterization of RAmKO and RImKO mice	37
Figure 2. Muscle of RAmKO mice show signs of a progressive dystrophy	39
Figure 3. Metabolic and structural properties diverge in skeletal muscle of RAmKO mice	41
Figure 4. Exercise performance and muscle physiology	43
Figure 5. Biochemical characterization	46
8. SUPPLEMENTAL FIGURES.....	47
Figure S1. Specificity of recombination and characterization of RAmKO mice	47
Figure S2. Expression pattern and assessment of muscular dystrophy parameters in RAmKO mice	49
Figure S3. Fiber size distribution and cytoskeletal architecture in RImKO mice	51
Figure S4. Subsarcolemmal accumulation of misshaped mitochondria and regionalized sIMHC expression in RAmKO mice	52
Figure S5. In-vivo and in-vitro alterations of Ser473-phosphorylated PKB/AKT, Mef2A and sIMHC.....	54
9. SUPPLEMENTAL TABLE	55
10. REFERENCES	57
11. CURRICULUM VITAE	64
12. ACKNOWLEDGEMENTS.....	66

1. SUMMARY

Growth of an organ during development and during adaptation in the adult can be controlled by alterations either in the number or the size of cells. The two mechanisms are fundamentally different and require distinct regulation. Rapamycin is a cell growth inhibitor used to treat a number of clinical indications including graft rejection and cancer. The molecular target of rapamycin is a Ser/Thr kinase, called TOR in yeast or mTOR in mammals. The evolutionarily conserved TOR pathway controls key aspects of cellular growth and metabolism. Among these are protein synthesis, ribosome biogenesis, nutrient transport and processing, autophagy and mitochondrial function. mTOR assembles into two distinct multiprotein complexes, termed mTORC1 and mTORC2. mTORC1 consists of raptor (regulatory associated protein of mTOR), mLST8 (mammalian lethal with SEC13 protein 8) and mTOR, and is sensitive to rapamycin. mTORC2 consists of rictor (rapamycin insensitive companion of mTOR), mSIN1, mLST8 (mammalian stress activated protein kinase interacting protein 1) and mTOR. As mTORC1 controls cell growth, it has also been implicated in the control of muscle mass. A vast array of genetic and pharmacological studies using rodent models supports this view. In contrast to the role of mTOR in growth, its metabolic readouts in skeletal muscle are poorly characterized. Little is also known of the function of rapamycin-insensitive mTORC2 whose primary readouts are thought to be the organization of the actin cytoskeleton. Recently, mTORC2 has also been proposed to be the essential kinase that phosphorylates PKB/AKT on Ser473.

To circumvent the early embryonic lethality of mice deficient for raptor (i.e. mTORC1) or rictor (i.e. mTORC2), we generated mice with floxed raptor or rictor alleles. Here we describe the phenotype of mice that lack functional mTORC1, mTORC2, or both complexes, specifically in skeletal muscle. We find that deletion of rictor does not cause an overt muscle phenotype. In contrast, raptor-deficient muscles manifest signs of atrophy and become progressively dystrophic. These muscles also display fundamental metabolic changes which involve impaired mitochondrial function. Furthermore, muscles display properties of fast-twitch, glycolytic skeletal muscle, but exhibit structural features and contraction properties indicative of slow-twitch, oxidative muscle fibers. These changes are either due to impaired activation of direct downstream substrates of mTORC1 or due to loss of negative feedback regulation of upstream components of the signaling pathway. Interestingly, this increased upstream signaling causes sustained hyperactivation of PKB/AKT, which is independent of mTORC2 kinase activity. Taken together, we provide unprecedented evidence for a crucial role of mTORC1 in the regulation of fundamental aspects of metabolism in a specific tissue. Furthermore we show that in the absence of negative feedback regulation from mTORC1 downstream components, mTORC2 is dispensable for PKB/AKT activation.

1.1 List of abbreviations

4E-BP1	eIF4E binding protein 1
AMPK	AMP activated protein kinase
Atg	atrogenes
ATM	ataxia telangiectasia mutated gene product
COX IV	cytochrome c oxidase IV
DmKO	double muscle knockout mice (raptor & rictor)
DNK-PK	doublestranded DNA dependent protein kinase
EDL	extensor digitorum longus (muscle)
eNOS	endothelial nitric oxide synthase
ERK	extracellular regulated protein kinase
FOXO	forkhead transcription factor
GLUT4	glucose transporter 4
GP	glycogen phosphorylase
GS	glycogen synthase
GSK-3	glycogen synthase kinase 3
GTPases	small guanosine triphosphatases
HSA	human skeletal actin
IGF-R	IGF receptor
IKK β	inhibitory κ B kinase β
ILK	integrin linked kinase
Inuslin-R	insulin receptor
MAFbx	muscle atrophy F-box / Atrogin-1
MDM2	murine double minute 2
Mef2A	myocyte enhancer factor 2A
MGF	mechano growth factor
MK2	MAPK activated protein kinase 2
mLST8	mammalian lethal with SEC13 protein 8
mSin1	mammalian stress activated protein kinase interacting protein 1
mTOR	mammalian target of rapamycin
mTORC1/2	mTOR Complex 1/2
MuRF-1	Muscle RING finger 1
NADH-TR	NADH tetrazolium staining
NEK6	NIMA related kinase 6
NFAT	nuclear factor of activated T cells
OXPPOS	oxidative phosphorylation
PAS	periodic acid schiff staining
PDK1/2	phosphoinositide dependent kinase 1/2
PGC-1 α	peroxisome proliferator activated receptor γ (PPAR γ) coactivator 1

PI3K	phosphoinositide 3 kinase
PIP3	phosphatidylinositol 3,4,5 trisphosphate
PKB/AKT	protein kinase B
PKC	protein kinase C
PRAS40	prolinerich Akt substrate 40
PRR5 / Protor	proline rich protein 5 / protein observed with rictor
PRR5L	PRR5-like protein
RAmKO	raptor muscle knockout mice
raptor	regulatory associated protein of mTOR
REDD1	protein regulated in development and DNA damage response 1
Rheb	Ras homolog enriched in brain
rictor	rapamycin insensitive companion of mTOR
RImKO	rictor muscle knockout mice
RTK	receptor tyrosine kinase
S6	40S ribosomal protein S6
S6K	S6 kinase
siMHC	slow myosin heavy chain
siTnI	slow isoform of troponin I
siTnT	slow isoform of troponin T
TNFR	tumor necrosis factor receptor
TNF α	tumor necrosis factor α
TSC1/2	tuberous sclerosis complex 1/2
YY1	yin yang 1

2. INTRODUCTION

2.1. Catching a glimpse of mTOR and its role in skeletal muscle

Loss of muscle mass can be due to many pathological conditions such as muscle dystrophy, AIDS, sepsis, burns, injuries or cancer. The wasting of muscle is not only a side effect of the primary disease but often contributes to morbidity. For example, cachexia is responsible for the deaths of ~22% of cancer patients [1]. Moreover, loss of muscle in the elderly contributes substantially to the loss of "quality of life" and the overall health costs [2]. Similarly, muscle contributes strongly to the metabolism of the entire body and it is well established that muscle exercise positively influences the outcome of metabolic disorders such as diabetes [3]. Although the medical need to treat muscle loss is obvious,

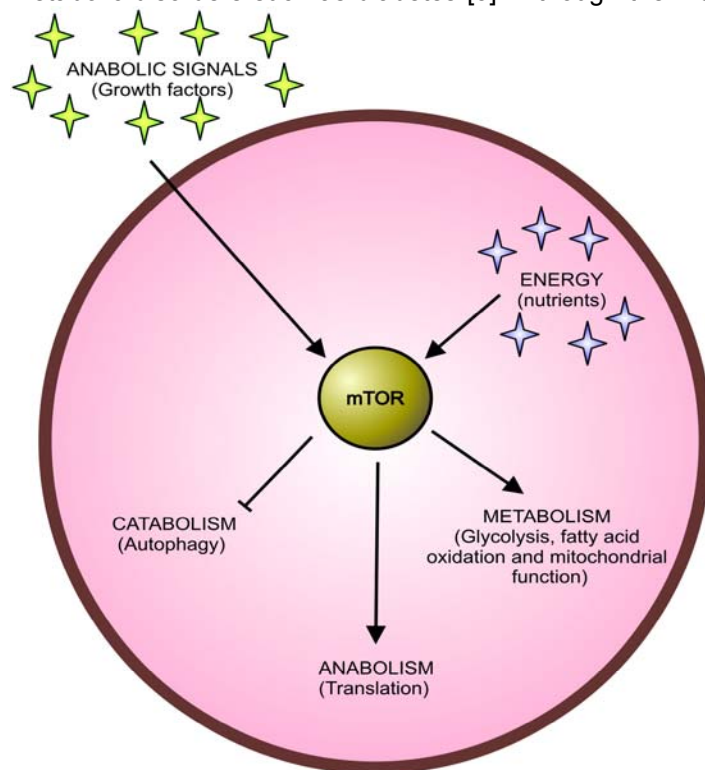


FIGURE 1. Proposed cellular functions of mTOR.

mTOR integrates positive environmental cues such as growth factors and nutrients and propagates anabolic signals into the cell. Catabolic processes are blocked whereas protein anabolism is fostered. Furthermore energy generation via mitochondria is facilitated by the activation of mTOR.

still little is known about the molecular mechanisms involved in regulating the plasticity of adult skeletal muscle.

2.1.1. mTOR mediated muscle growth

In the past years, evidence has accumulated that the mTOR signaling pathway is likely to be one of the effector pathways involved in controlling postnatal muscle plasticity. The scientific basis for this role of mTOR is the finding that both upstream and downstream components of mTOR have been shown to control muscle mass in rodents. For example, the main activators of mTOR, insulin-like growth factor-1 (IGF-1) and protein kinase B (PKB; also called AKT) are both involved in this process. Transgenic mice that overexpress IGF-1 in skeletal muscle have bigger muscles

and mice deficient in PKB/AKT have smaller organs including muscle fibers [4, 5]. Furthermore, constitutively active forms of PKB/AKT can induce profound muscle hypertrophy in mice [6-8]. Interestingly, pharmacologic blockade of mTOR prevents PKB/AKT mediated muscle hypertrophy in these animals [6]. Beyond the evidence from studies on IGF-1 or PKB/AKT, overexpression of TSC1, an upstream inhibitor of mTOR, and inactivation of the mTOR downstream target S6K, cause muscle atrophy in mice [9, 10]. Furthermore, pharmacological inhibition of mTOR prevents hypertrophy of soleus muscles during synergistic ablation and recovery from muscle atrophy after hind limb

suspension [8]. In summary, genetic and pharmacologic studies in rodents point out that mTOR has a crucial role in the regulation of skeletal muscle mass. Nevertheless, because of early embryonic lethality, direct evidence in form of a mTOR knockout mouse is still missing [11-13].

Next to experimental evidence from studies with rodents, also in humans, activation of the PKB/AKT/mTOR pathway has been shown to positively influence skeletal muscle mass. Most of these studies made use of the effects of growth hormone (GH). Systemic application of GH leads to increased circulating levels of IGF-1 from the liver and other tissues [14]. GH also leads to local synthesis of IGF-1 in the respective tissues, where it then acts in a paracrine fashion to activate mTOR [14]. These effects have been exploited to treat several pathologic states in humans that are accompanied by muscle wasting. For example, GH and/or IGF-1 have been used to treat patients with HIV dependent muscle wasting. Such treatment results in significant increases in lean body mass [15, 16]. Also after severe trauma and burns, muscle protein catabolism is increased in humans [17, 18] and application of GH can efficiently counteract these changes [19-21]. Sarcopenia, the loss of muscle in the elderly, is another example for a pathologic situation in which pharmacologic GH and/or IGF-1 intervention could be beneficial [22]. Ageing correlates with declining secretion of GH and IGF-1 which further emphasizes the potential usefulness of such a treatment [23, 24]. Nevertheless, it is not yet established whether elderly people finally profit from GH replacement [25]. The downside of GH substitution in patients are adverse effects, for example increased tumor growth [26]. It has been proposed that mainly the increase in circulating IGF-1 levels upon GH substitution triggers tumor development and metastasis [27]. Therefore, understanding of the growth effects of non-systemic, locally acting IGF-1 is of profound importance and could particularly facilitate the treatment of muscle wasting that accompanies certain cancers. More knowledge on the tissue specific, paracrine effects of IGF-1 could help to “locally” activate the involved signaling pathways, while preventing systemic side effects.

2.1.2. Nutrients and mTOR

Next to its function in growth, mTOR has also been shown to be a cellular integrator of nutrient availability. Nutrients can activate mTOR directly and indirectly. In higher organisms, increases in systemic glucose trigger the release of the anabolic hormone insulin from the pancreatic islets which activates mTOR via the insulin receptor [28, 29]. Amino acids in turn, can directly activate the kinase via small guanosine triphosphatases (GTPases) [30]. Withdrawal of most amino acids in cell culture inactivates mTOR, but withdrawal of leucine alone is as suppressive as withdrawal of all amino acids [31]. This suggests a primacy of leucine in regulating mTOR. Interestingly, supplementation with a mixture of amino acids particularly rich in leucine, counteracts age-induced muscle loss in rats. These effects correlate with an increased activation of mTOR in muscles of these animals [32]. Initially based on empirical experience, it is known for almost 30 years that branched chain amino acids (BCAA's: leucine, valine and isoleucine) supplementation before and after exercise have beneficial effects on muscle by decreasing exercise-induced damage and promoting protein synthesis [33]. Again, BCAA supplementation in humans is accompanied by increased mTOR signaling [34].

2.1.3. mTOR balances cellular energy generation

The cellular ATP/AMP levels are sensed via the AMP-activated protein kinase (AMPK) which is an upstream regulator of mTOR [35]. Therefore, both nutrient availability and the energy status of the cell converge on mTOR. Consistent with a role in integrating nutrient and energy availability, mTOR regulates glycolytic and oxidative phosphorylation (OXPHOS) genes in a positive manner [36-40]. Because of its role in the regulation of OXPHOS, mTOR has also been proposed to indirectly regulate the cellular fatty acid content [40]. mTOR's effects on mitochondrial function seem to be mediated by an interacting protein called Peroxisome proliferator-activated receptor γ (PPAR γ) coactivator 1 (PGC-1 α). PGC-1 α is a transcription factor that has a key role in regulating mitochondrial function by directly triggering the transcription of OXPHOS genes [41]. Loss of mTOR has been shown to lower the levels of PGC-1 α and the expression of its target genes [40]. Because of its role in facilitating mitochondrial function and biogenesis, PGC-1 α has been proposed to be involved in adaptations to endurance exercise [42]. Such types of exercise can increase the mitochondrial content and therefore the oxidative capacity of muscle fibers. Adaptations of skeletal muscle towards a more aerobic energy utilization have been demonstrated to have potent beneficial effect in many diseases [43]. An increase in mitochondrial content is accompanied by a slower utilization of muscle glycogen and blood glucose, a greater reliance on fat oxidation, and lowered lactate production [44]. The above mentioned findings on the regulation of OXPHOS by mTOR strongly suggest that this kinase is involved in adaptations to exercise. Indeed, in humans the mTOR signaling pathway is responsive to acute exercise and short-term intensified endurance training [45].

2.1.4. mTOR regulated autophagy

mTOR has also been connected to the process of autophagy. This catabolic mechanism involves the import and breakdown of cytoplasmic components into the lysosome ensuring amino acid availability for de novo protein synthesis and, depending on the tissue, for gluconeogenesis. The mechanism of autophagy has been connected to muscle wasting [46]. As discussed above, activation of mTOR can prevent muscle atrophy, which suggests that this effect could be mediated by inhibition of autophagic processes [8]. Despite of extensive research, the molecular mechanisms by which mTOR regulates autophagy remain to be determined [47]

2.1.5. Bottom line on the role of mTOR in skeletal muscle

Taken together, experimental evidence currently indicates that mTOR functions as a central hub that coordinates and integrates anabolic signals from the exterior of the muscle fibers to the cellular energy plants and the growth machinery. mTOR can be considered as a cellular switch that is activated by increased fuel, such as glucose, amino acids, and by growth factors, such as IGF-1 and insulin. Once in the on-state, this switch increases energy production via glycolysis and the use of mitochondria. Increased energy stores are a prerequisite for the subsequent building up of proteins via increased translation. Next to driving the whole cell into the anabolic program, mTOR also blocks catabolic processes, such as autophagy. It is therefore beyond question that this central role of mTOR in the cell

makes it a very interesting target for the development of drugs to counteract diseases that are accompanied by wasting and metabolic imbalance.

2.2. The PKB/AKT and mTOR signaling pathway

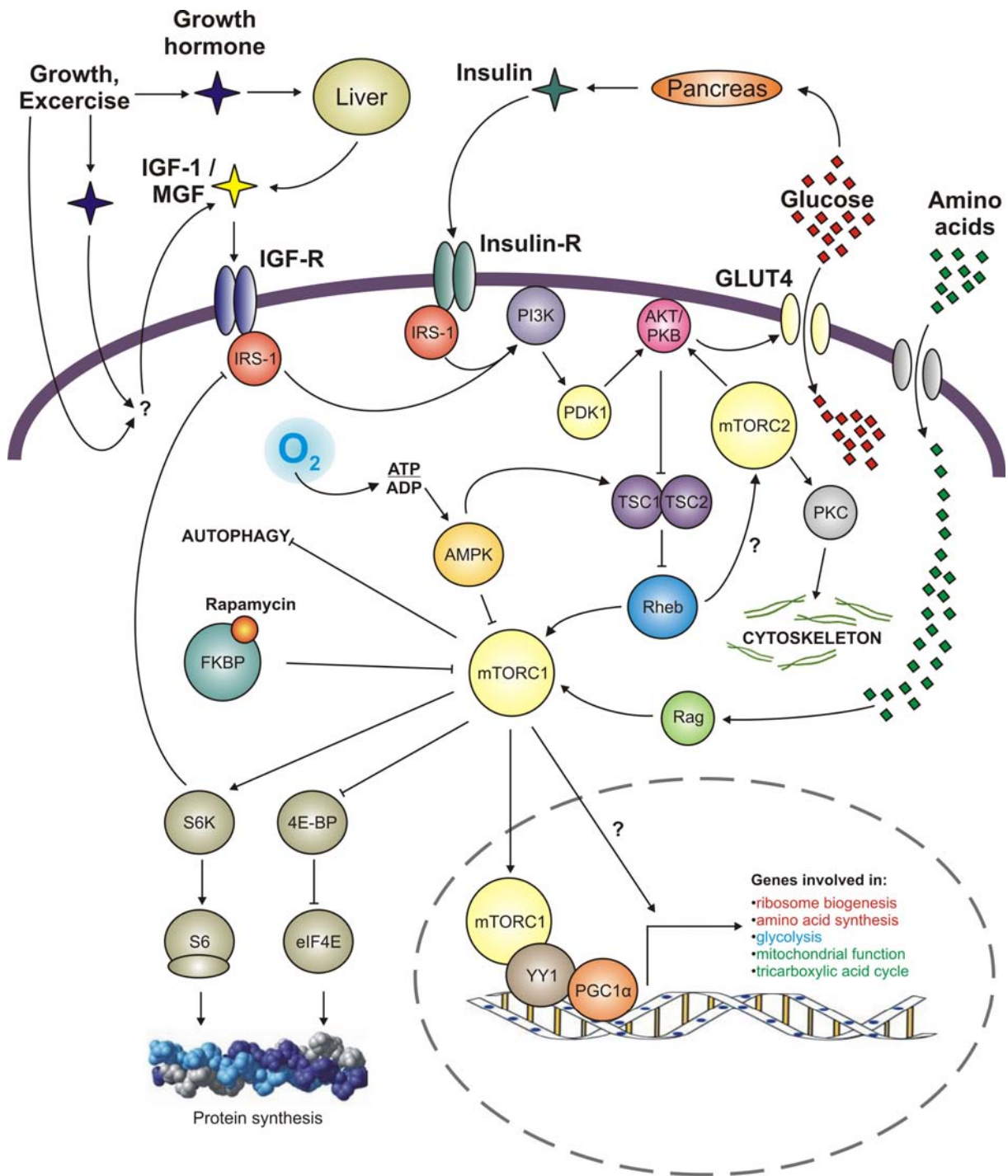


FIGURE 2. The insulin and mTOR signaling pathways.

mTOR complex 1 mTORC1 and possibly mTORC2 respond to growth factors, energy status of the cell and nutrients. Activation of mTORC1 triggers translational processes and the transcription of metabolic genes, whereas mTORC2 acts on the cytoskeleton.

One way of regulating mTOR in the postdevelopmental stage in mammals is via the PKB/AKT/IGF-1 pathway. For example, in response to exercise, GH is released from the anterior pituitary gland into the circulation. As discussed under 2.1.1., GH subsequently acts on the liver and other tissues to cause the release of systemic insulin-like growth factor [14]. Alternatively GH and/or exercise also

causes the release of a muscle tissue specific splice variant of IGF-1, the so called mechano growth factor (MGF) [48, 49]. Augmenting the effect of the systemic growth factors, the local, muscle released MGF and IGF-1 act back on the tissue in a paracrine manner. The highly anabolic hormone insulin in turn, is released exclusively in an endocrine manner by the pancreas in response to glucose [28]. Therefore, muscle growth is regulated both, locally by IGF-1 and MGF as well as systemically by GH, insulin and IGF-1. The insulin and the IGF receptor (Insulin-R and IGF-R) are very similar in structure and function. Binding of insulin or insulin-like growth factors IGFs to their receptors leads to recruitment and phosphorylation of the insulin receptor substrate (IRS) and activation of the PI3K cascade [50]. Protein kinase B (PKB), also known as AKT, is subsequently recruited to the membrane and becomes activated. Activation of PKB/AKT cause the membrane insertion of glucose transporter 4 (GLUT4) which facilitates the uptake of glucose into the cell [51-53]. Activation of PKB/AKT triggers the inactivation of the tuberous sclerosis complex 1 (TSC1) and 2 (TSC2) to release their inhibition of Ras homolog enriched in brain (Rheb), which, in turn, activates mTOR [54]. Besides insulin and IGF, amino acids have been shown to activate the mTOR pathway via Rag proteins, a family of four related small guanosine triphosphatases [55]. Furthermore, TSC1/2 and mTORC1 have been shown to be phosphorylated by AMPK which is directly regulated by the cellular ATP content and indirectly by the availability of oxygen [56].

In mammals, mTOR forms two distinct complexes. Activation of mTOR Complex 1 (mTORC1) leads to an increase in translation via activation of S6K and inhibition of the translation inhibitor 4E-BP [57]. Furthermore mTORC1 interacts with yin-yang 1 (YY1) and PGC-1 α , which is a main transcriptional regulator of OXPHOS genes [58]. mTORC1 can be blocked by the immunosuppressive drug rapamycin. This compound inhibits the complex by acting on it via FK506-binding protein 12 (FKBP12). Activation of mTORC2 in turn, induces phosphorylation of PKC and influences the actin cytoskeleton [59, 60]. mTORC2 has also been proposed to be an upstream kinase for PKB/AKT.

2.3. mTOR complex 1 and 2

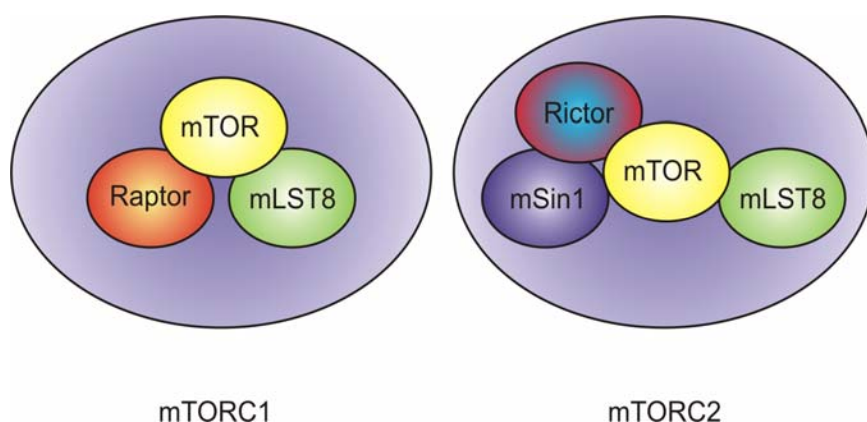


Figure 3. The mTOR complexes.

In mTORC1, the mTOR catalytic subunit associates with raptor and mLST8 (also known as GβL). mTORC2 in contrast, contains instead of raptor a protein called rictor, but also other subunits such as mLST8 and mSin1.

The two abovementioned distinct TOR complexes in mammals were identified from collaborating work of our laboratory with that of Prof. Michael N. Hall (Biozentrum, University of Basel) [59]. mTORC1 consists of mTOR, mLST8 and raptor and is rapamycin sensitive. Raptor was identified as an mTOR binding partner that mediates mTOR signaling to its targets [61-63]. Raptor recruits mTOR to substrates, including 4E-BP1 and S6K, through their TOR signaling TOS motifs and is required for mTOR-mediated phosphorylation of these substrates [64-66]. It has been suggested that one possible mechanism for the inhibition of mTORC1 by FKBP12-rapamycin is its competition for binding with raptor [67]. The mTOR-raptor interaction and its regulation by nutrients and/or rapamycin is also dependent on mLST8 [61, 68]. More recently PRAS40 was identified to be an upstream negative regulator of mTORC1 [69, 70]. PRAS40 can bind to mTORC1 via raptor and seems to regulate it negatively by functioning as a direct inhibitor of substrate binding [69, 70].

In mTORC2, which is largely rapamycin insensitive, rictor and mLST8 mediate mTOR signaling to downstream targets including PKC α [61]. Furthermore, the rictor-mTOR complex has been shown to phosphorylate PKB/AKT on Ser473 and is thus proposed to be the equivalent for PDK2, facilitating phosphorylation of Akt/PKB on Thr308 by PDK1 [71]. Both rictor and another component unique to mTORC2 called mSin1 are necessary for the phosphorylation of PKB/AKT [59, 60, 72]. mTORC2 has been suggested to exist in several isoforms that are defined by different splice variants of mSin1 [72]. Another protein, called PRR5 (Proline-rich protein 5) or protor (protein observed with rictor), was recently identified to bind to rictor independently of mTOR [73, 74]. PRR5/protor expression seems to be controlled by rictor and its loss does not significantly reduce phosphorylation of PKB/AKT at Ser473. Therefore, the function of the PRR5/protor-mTORC2 interaction remains to be determined. Furthermore, a PRR5-like protein (PRR5L) was identified to bind to mTORC2 but is not required for mTORC2 integrity [69]. PRR5L seems to dissociate from mTORC2 in cells with active mTOR signaling to induce apoptosis. Loss of PRR5L can also prevent apoptosis in mTORC2 deficient cells. Thus, PRR5L can be considered to be a downstream effector of mTORC2. Different from the raptor-mTOR association, the interaction between mTOR and rictor is not regulated by upstream signals. The

mechanism that induces mTORC2 kinase activity is not yet understood. However, some evidence suggests that TSC1/2 also regulates mTORC2 [75]. Germline disruption of mTOR and raptor in mice causes embryonic lethality around implantation [11, 13, 76]. Rictor knockout in contrast, leads to lethality in later developmental stages [12].

2.4. Protein kinase B / AKT

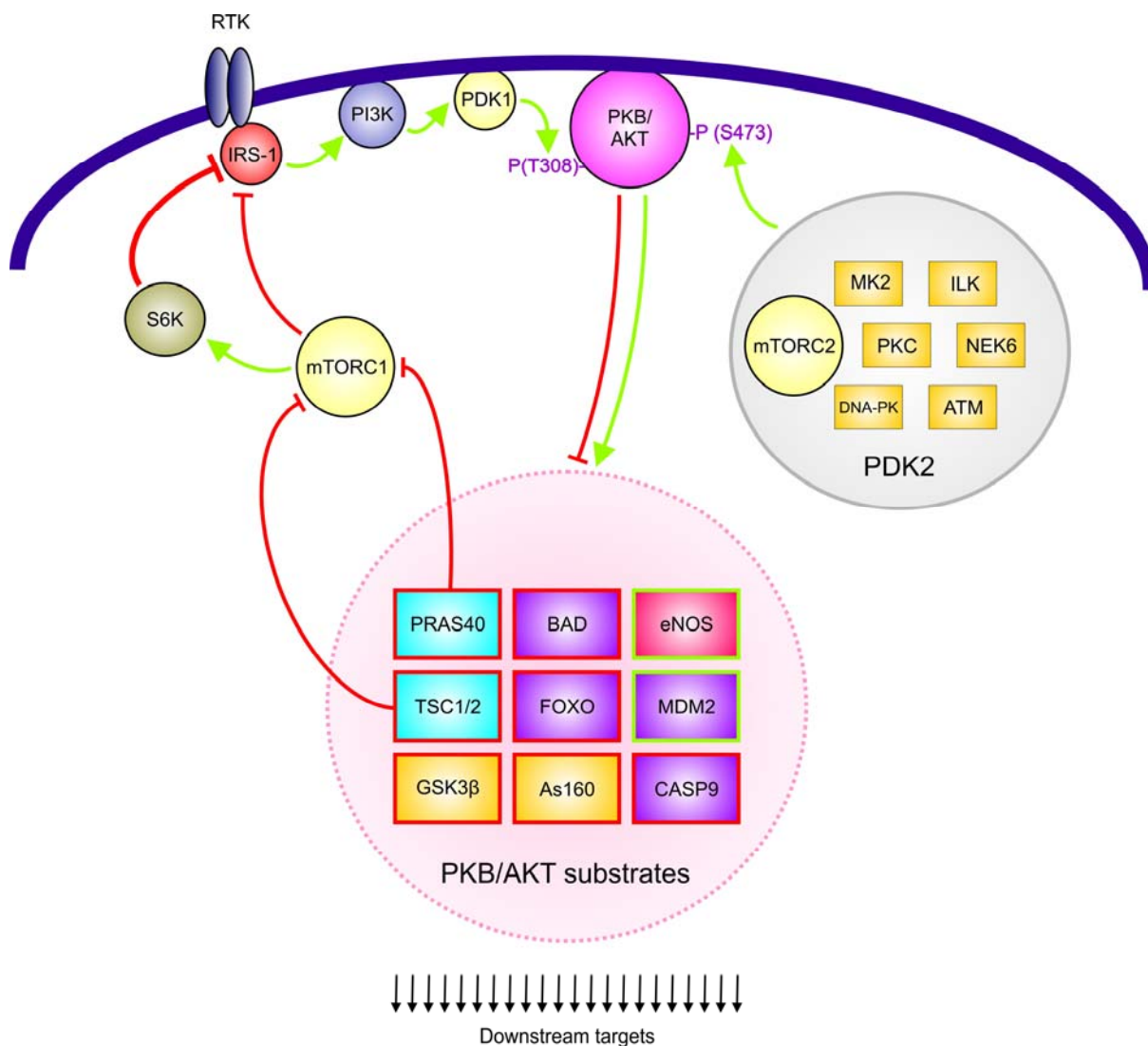


Figure 4. Protein kinase B or AKT

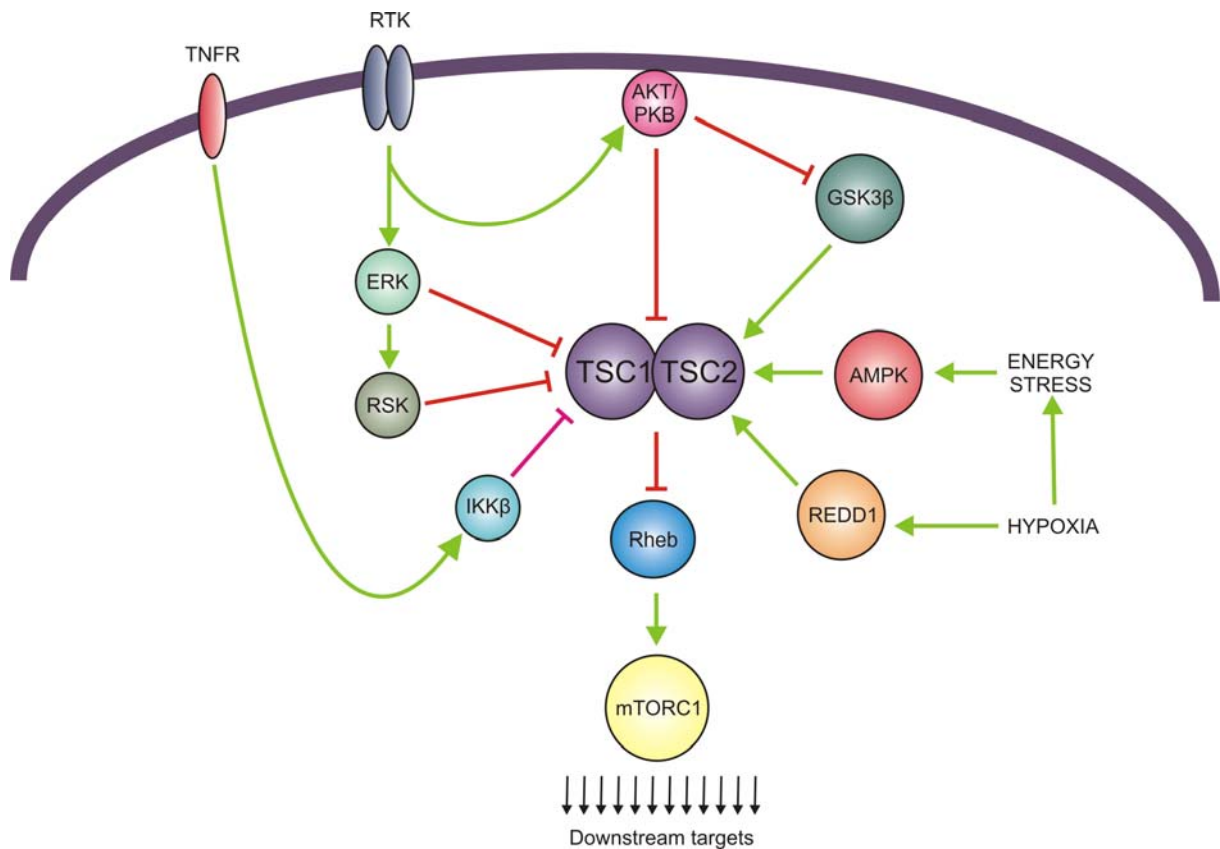
As a consequence of PI3K activity PKB/AKT is recruited to the membrane where PDK2 phosphorylation stimulates the subsequent phosphorylation by PDK1. PKB/AKT can subsequently activate manifold cellular targets that can mediate e.g. survival, growth, proliferation, glucose uptake, metabolism, and angiogenesis. Activating interactions are indicated by green lines, whereas inactivating interactions are symbolized by red lines.

As discussed in 2.1.1. and 2.2., the mTOR upstream component PKB/AKT is a central component of the pathway which mediates growth of muscle fibers [8]. PKB/AKT possesses a protein domain known as a PH domain that can bind to phosphatidylinositol 3,4,5-trisphosphate (PtdIns3,4,5P3 or PIP3) that is generated by a family of enzymes called phosphoinositide 3-kinases (PI3K) [77]. Activation of a receptor tyrosine kinase (RTK) such as the insulin-R causes PI3K to generate elevated PIP3 levels which recruit PKB/AKT to the membrane. Once correctly positioned at the membrane PKB/AKT can then be phosphorylated by phosphoinositide dependent kinase 1 (PDK1) at threonine 308 and (PDK2) at serine 473 [77]. So far, at least 10 kinases have been suggested to function as PDK2. These include MAPK activated protein kinase 2 (MK2), integrin-linked kinase (ILK), PKC, the NIMA-related

kinase-6 (NEK6), the doublestranded DNA-dependent protein kinase (DNA-PK), and the ataxia telangiectasia mutated gene product (ATM) [78]. Recently, mainly emphasized by the Sabatini laboratory, mTORC2 has been proposed to be the long-sought PDK2 [71]. Despite of that, there is evidence in the literature that mTORC2 is not solely required for PKB/AKT phosphorylation (see discussion under 2.7.) [12, 79].

Searching the literature reveals over 100 reported Akt substrates [80]. Most importantly in the context of mTOR signaling, PKB/AKT associates with the TSC1/2 complex, promoting phosphorylation of TSC2 and increased degradation which leads to the activation of mTORC1 [81-86]. Furthermore, PKB/AKT can phosphorylate and inhibit the mTORC1 upstream inhibitor PRAS40 [87]. Therefore, inactivation of mTORC1 upstream inhibitors seems to be a general mechanism of mTORC1 activation by PKB/AKT. Pointing out a crucial role of PKB/AKT in glucose metabolism, its activation facilitates the insulin-induced, AS160 (also known as TBC1 domain family member 4; TBC1D4) dependent, translocation of GLUT4 to the plasma membrane and inhibits glycogen synthase kinase 3 (GSK-3) which results in promotion of glycogen synthesis [51-53, 88]. PKB/AKT has also been shown to regulate cellular survival by binding and regulating Forkhead transcription factors (FOXO), Bcl-2 family proteins, murine double minute 2 (MDM2) and caspase-9 [89-93]. Furthermore, a crucial role of PKB/AKT in angiogenesis and tumor development has emerged [94]. For example, PKB/AKT directly activates endothelial nitric oxide (NO) synthase (eNOS) which is involved in carcinogenesis [95-97]. Interestingly, constitutive activation of Akt in skeletal muscle *in vivo* is sufficient to induce rapid skeletal muscle hypertrophy and loss of adipose tissue [98]. These effects correlate with a sustained activation of p70S6 kinase and are rapamycin sensitive which suggests an involvement of mTOR [6].

2.5. The tuberous sclerosis complex



The TSC1/2 complex

TSC1/2 complex integrates multiple activating and inhibitory signalling pathways to regulate mTORC1 activity. Activating interactions are indicated by green lines, whereas inactivating interactions are symbolized by red lines.

Downstream of the PI3K–PKB/AKT pathway, TSC1/2 is suggested to be the primary negative regulator of mTORC1 signaling. In mammalian cells mTORC1-mediated phosphorylation of both S6K and 4E-BP1 is inhibited by TSC1/2 complex overexpression and is activated independently from growth factors in cells lacking the TSC1/2 complex [84, 85, 99-103]. Overexpression of a human TSC1 transgene in mouse skeletal muscle leads to stabilized endogenous TSC2, inhibition of the mTOR signaling and a reduction of muscle mass [10]. Furthermore, it was demonstrated that the TSC1/2 complex directly regulates the small GTPase Ras homolog enriched in brain Rheb which activates mTORC1 [104-107]. TSC2 has a GAP domain which stimulates the GTPase activity of Rheb [104, 105]. Activation of the extracellular regulated protein kinase (ERK) and its downstream target 90 kDa ribosomal S6 kinase (p90rsk or RSK) can also inhibit TSC1/2 and stimulate mTORC1 activity. Growth stimuli that predominantly activate ERK, but not PI3K, such as the phorbol ester PMA, seem to modulate mTORC1 signaling through phosphorylation of the TSC2 complex [108, 109]. Interestingly, also the pro-inflammatory cytokine tumor necrosis factor α (TNF α) has been found to stimulate mTORC1 signaling through inhibitory κ B kinase β (IKK β) which can associate with TSC1 and phosphorylates it [110]. As discussed before, phosphorylation of TSC2 by AMPK modulates mTORC1 according to the status of intracellular ATP [56, 111]. AMPK inhibits mTORC1 under nutrient deprivation, at least in part, by phosphorylating and activating TSC2. This phosphorylation seems to

prime TSC2 for further phosphorylation by GSK3 β [112] which is regulated downstream of PKB/AKT and frizzled receptors [88, 113]. Next to low ATP levels, conditions of oxygen depletion (i.e. hypoxia) activate the TSC1/2 complex and block mTORC1 signaling [114]. This effect is mediated indirectly via decreased OXPHOS resulting in low ATP levels that activate AMPK, and directly by protein regulated in development and DNA damage response 1 (REDD1) which seems to reverse Akt-mediated inhibition of TSC1/2 under hypoxic conditions [115]. In conclusion, the TSC1/2 complex modulates mTORC1, dependent on the presence of growth factors and inflammatory cytokines but also according to the cellular oxygen level and the energy status of the cell.

2.6. Downstream targets of mTORC1

Two well known targets of mTORC1 are S6K and 4E-BP1. In response to amino acids and growth factors, mTORC1 activates S6K, which in turn, phosphorylates the 40S ribosomal protein S6 (S6) and triggers protein synthesis [116, 117]. Inactivation of S6K in mice causes muscle atrophy that is independent of changes in global translation, expression of E3 ubiquitin ligases and autophagy, suggesting the activation of an uncharacterized mediator of muscle atrophy [9, 118]. Furthermore S6K knockout mice are resistant against diet induced obesity [119]. Genes such as PGC1 α which control mitochondrial function are upregulated in adipose tissue of S6K knockout mice. This is probably the reason for the increased mitochondrial number as well as for the upregulation of genes involved in uncoupling of the mitochondrial proton gradient [119]. mTORC1 also phosphorylates 4E-BP1, inducing its dissociation from eIF4E, which can bind the cap structure at the 5'-termini of mRNA and thereby facilitates cap-dependent translation [120]. Interestingly, 4E-BP1 knockout mice manifest a phenotype that reiterates aspects of S6K knockout mice concerning adipose tissue. Such animals contain less fat and increase the expression of PGC1 α and of uncoupling proteins [121]. The adipose tissue phenotype observed in S6K and 4E-BP knockout mice seems to be similar in many aspects. This could be due to alterations in the levels of a circulating factor from another organ. Alternatively, S6K and 4E-BP could have a common or functionally redundant downstream effector in adipocytes. Another possibility is that loss of either S6K or 4E-BP increases the levels of mTORC1 acting on different substrates, for example on positive regulators of mitochondrial function such as PGC1 α . Furthermore, it can not be excluded that loss of S6K or 4E-BP could lead to hyperactivation of the upstream pathway due to decreased negative feedback regulation. This, in turn, could lead to activation of mTOR and increased PGC1 α expression and/or activity.

It is known for a long time that TOR-controlled protein synthesis in yeast involves transcriptional regulation of genes that control ribosome biogenesis [54]. Both, in yeast and mammalian cells, rapamycin causes a decrease in the levels of genes involved in de novo biosynthesis of lipids and nucleotides, glycolysis, translation initiation and elongation, and tRNA synthesis, and an increase in genes involved in oxidizing amino acids and fatty acids and nucleotide salvage pathways [37, 38, 122]. Genes involved in mitochondrial function in turn respond differently to the drug in the two systems. In yeast, rapamycin significantly upregulates genes required for cell respiration, while, in most mammalian cell lines, rapamycin down-regulates genes essential for mitochondrial function [36, 40, 122, 123]. However, with rare exceptions, the molecular mechanisms of transcriptional regulation by mTOR remain largely unexplained. Interestingly, complex formation between mTOR and raptor has been correlated with overall mitochondrial activity [39] and, as also discussed under 2.1.3. and 2.2., a recent report demonstrated that mTORC1 can interact with a protein called YY1 and PGC1 α , a key transcription factor of mitochondrial genes [40]. This study suggests that decreased mTOR activity inhibits an YY1–PGC1 α interaction, resulting in a decreased expression of mitochondrial genes, including PGC1 α itself. Interestingly, neither knockdown of S6K nor inhibition of PKB/AKT lowered PGC1 α and YY1 expression in this study.

2.7. Downstream targets of mTORC2

It has been shown in yeast that TORC2 can signal through a Rho-type GTPase on PKC which modulates the actin cytoskeleton [61]. Loss of rictor in some mammalian cell lines also leads to changes in the organization of the actin cytoskeleton [59, 60] and mTORC2 is also able to activate PKC in such cells [60]. PKC α is expressed in a broad range of tissues and seems to be involved in many cellular processes like cell growth, cell cycle control, and the regulation of cell shape and motility [124]. Interestingly, rictor knockout mice develop normally until day E9.5 which requires motile cells with an intact actin cytoskeleton [12]. This also suggests that the prenatal function of mTORC2 is only required late in development. As discussed under 2.4, activation of PKB/AKT requires its recruitment to the plasma membrane, where it is phosphorylated on Ser473 by PDK2, and on Thr308 by PDK1. In embryonic fibroblast derived from rictor knockout mice, phosphorylation of Ser473 is drastically reduced which lead to the suggestion that mTORC2 is the upstream kinase for PKB/AKT [71]. However, in other studies residual Ser473 phosphorylation is detected in such cells [12, 79]. This suggests that mTORC2 is not the only kinase required for Ser473 phosphorylation on PKB/AKT. Furthermore, GSK3, TSC2, mTOR, S6K and 4E-BP, which are widely accepted Akt/PKB targets, are not affected by the loss of functional mTORC2 [125]. Only forkhead transcription factors, namely FOXO1, FOXO3 and FOXO4, phosphorylation is reduced upon loss rictor. Therefore, mTORC2 activity is only required to regulate a subset of PKB/AKT substrates [12, 71, 125, 126].

2.8. The negative feedback from S6K

Chronic insulin stimulation leads to the proteasomal degradation and to downregulated transcription of the adaptor protein IRS-1 [127-133] due to negative feedback regulation of the insulin / PI3K signaling pathway. Furthermore, loss of the TSC complex results in impaired activation of PKB/AKT upon insulin which has been shown to be due to transcriptional repression of the IRS-1 gene [134, 135]. Next to transcriptional repression, the mTORC1 downstream target S6K can phosphorylate IRS-1 on specific residues which prevents its recruitment and binding to RTKs [134, 136]. Under some conditions, mTOR itself is able to phosphorylate and inhibit IRS-1 [137, 138]. In line with these findings, mTORC1 inhibition with rapamycin can induce PKB/AKT activation in a variety of cancer cell lines [139-141].

3. RESULTS

3.1. Skeletal muscle-specific ablation of raptor and rictor

To examine the function of mTORC1 and mTORC2 in skeletal muscle we used the Cre-loxP recombination system. To this end, we introduced loxP sites into the raptor and the rictor locus (Figure 1A). In both cases, Cre-mediated recombination causes a frame shift and early stop of translation. In addition, FRT sites were inserted that flanked a neomycin resistance cassette for the selection of targeted embryonic stem ES cells. This cassette was removed using Flp deleter mice (Figure 1A; [142]). Southern blot analysis confirmed successful targeting in ES cells and germ line transmission of resulting chimeras (Figure 1B). Mice homozygous for the floxed allele *raptor^{fl/fl}* or *rictor^{fl/fl}* were mated with heterozygous floxed mice that also expressed Cre recombinase under the control of the muscle-specific human skeletal actin (HSA) promoter [143]. Mice positive for the HSA-Cre transgene that also carried two floxed alleles were then analyzed. For simplicity, we refer to HSA-Cre; *raptor^{fl/fl}* as RAmKO (for raptor muscle knockout) and to HSA-Cre; *rictor^{fl/fl}* as RImKO (for rictor muscle knockout mice). Successful recombination of raptor or rictor was confirmed by PCR on genomic DNA isolated from tibialis muscle (Figure S1A). Western blot analysis of RAmKO and RImKO skeletal muscle revealed a strong reduction of the respective proteins (Figure 1C; Figure S1B and Table S1). Residual expression of these proteins in knockout muscle is not due to leaky recombination of the targeted allele as *raptor^{fl/fl}* or *rictor^{fl/fl}* mice crossed to other Cre-expressing mice led to a complete loss of the respective protein in the targeted tissue (Figure S1B; [144]; M.N. Hall, personal communication). Thus, the low levels of raptor and rictor protein that were detected in the RAmKO and RImKO muscles are ascribable to the expression of raptor or rictor in non-targeted cells, such as fibroblasts, satellite cells, Schwann cells and peripheral nerves, which are also contained in skeletal muscle.

Neither RAmKO nor RImKO mice showed an overt phenotype in the first weeks of life. Starting at the age of approximately 5 weeks, RAmKO mice could be distinguished from their littermates by their lower body weight. The difference became significant after day 63 and the mice remained lighter throughout life (Figure 1D). In contrast, the body weight of RImKO mice did not differ significantly from controls, although at higher age RImKO mice were slightly heavier (Figure 1D). For both RAmKO and RImKO mice, the food consumption was comparable to controls (Figure S1C and data not shown). RAmKO mice developed a pronounced kyphosis starting at the age of approximately 2 months and became markedly lean (Figure 1E; Figure S1D). In contrast, RImKO mice appeared normal. Finally, RAmKO mice began to die at the age of 110 days and none survived for more than 190 days (Figure 1F). RImKO mice did not die prematurely the oldest RImKO mice now being more than 2 years old.

To examine whether the difference in weight gain was based on reduced muscle mass in RAmKO mice, we weighed different muscles and several other organs at day 90 i.e. before the mice showed a severe phenotype and at day 140. As shown in Table 1, all the muscles measured were significantly lighter in 90 and 140 day-old RAmKO mice compared to controls. As RAmKO mice appeared lean

(Figure 1E) and only little or no fat was detected in older mice (Figure S1D), we also weighed the epididymal fat pads. Indeed, RAmKO mice contained significantly less adipose tissue at the age of 140 days Table 1. The loss of adipose tissue does not seem to be due to changes in mitochondrial uncoupling properties as the body temperature of RAmKO mice was not different from control littermates (Figure S1E). The weight of the liver was indistinguishable from controls whereas hearts were again lighter Table 1. The left ventricle mass of the heart, however, correlated with the difference in body weight (Figure S1F), indicating that the difference in heart weight is probably due to allometric scaling [145]. Moreover, the ejection fraction determined by echocardiography was indistinguishable from littermate controls data not shown. Finally, we could not detect any recombination events in the hearts of RAmKO mice (Figure S1A). Our data therefore show that raptor deficiency in skeletal muscle causes a progressive, disproportional loss of skeletal muscle and fat.

3.2. Deficiency of mTORC1 but not mTORC2 causes muscle dystrophy

Kyphosis and early death are often signs of muscle dystrophy [146]. We therefore examined different skeletal muscles of RAmKO and RImKO mice using hematoxylin & eosin H&E staining. No change in the overall architecture of soleus and extensor digitorum longus EDL muscle was found in RImKO mice (Figure 2A). Muscles from RAmKO mice showed signs of a dystrophy, such as mononuclear cells (green arrowheads) and a high number of small and large muscle fibers (blue arrowheads). In soleus muscle and to a lower extent in EDL, we also found muscle fibers with centralized nuclei (white arrowheads), indicative of ongoing de- and regeneration, and structures reminiscent of central cores (black arrowheads in Figure 2A and Figure 2B). Quantification showed that the fiber size distribution was strongly altered in both soleus and EDL muscle (Figure 2C, D, E, and F). In addition, the number of centralized myonuclei (Figure 2G) and the relative percentage of muscle fibers with the central core-like structures (Figure 2H) was higher in RAmKO mice compared to controls. Dystrophic hallmarks seemed more pronounced in soleus than in EDL muscle. Interestingly the severity of the dystrophy correlated with the high endogenous expression of raptor, rictor, mTOR or PKB/AKT in wild-type soleus muscle (Figure S2A). Muscles of RAmKO mice also showed increased immunoreactivity for tenascin-c and f4/80 (Figure S2B), which mark fibrotic tissue [147] and infiltrating macrophages [148], respectively. However, other dystrophic hallmarks including increased uptake of Evans blue into muscle fibers and increased levels of creatine kinase in the blood could not be detected (Figure S2C) and data not shown. Similarly, the number of muscle fibers was not changed in soleus muscle of RAmKO mice compared to controls (Figure S2D). Neuromuscular junctions of RAmKO mice were indistinguishable from those in control mice (Figure S2E). Probably due to ongoing de- and regeneration, many extrasynaptic acetylcholine receptor AChR clusters could be detected in the diaphragm of RAmKO mice (Figure S2F). Based on the extensive muscle wasting and the high degree of fibrosis, the dystrophy was particularly severe in the diaphragm of older mice (Figure 2I), suggesting that respiratory failure might be the cause of premature death. In contrast to RAmKO mice, muscles of RImKO mice did not show any alterations in fiber size (Figure S3A) and in the cytoskeletal organization as indicated by the sarcomeric arrangement of α -actinin (Figure S3B). In summary, our data show that ablation of raptor and thus of mTORC1, but not of rictor, results in a progressive muscle dystrophy.

3.3. Skeletal muscles of RAmKO mice show alterations in their metabolic and structural properties

One of the first observations we made during the course of this work was that muscles of RAmKO mice appeared paler than those of RImKO or control mice. This difference was particularly striking for the soleus muscle (Figure 3A), arrowhead and was not based on decreased vascularization, as revealed by staining for laminin- α 5 data not shown, which is expressed in blood vessels [149]. To test for changes in mitochondrial function, we used an NADH-tetrazolium (NADH-TR) staining. Indeed, the activity of oxidative enzymes appeared lower in both, EDL and soleus muscle of RAmKO mice (Figure 3B). Fibers with central core-like structures, which were completely devoid of NADH-TR reactivity, could be found in RAmKO soleus muscle (black arrowheads). Such a lack of NADH staining is a diagnostic feature of central core disease [150]. To further test whether the changes in NADH-TR reactivity involved mitochondria, we also examined longitudinal sections of soleus muscle by electron microscopy. Muscle of RAmKO mice was distinguishable from control muscle by a substantial loss of intermyofibrillar mitochondria, which are normally localized perpendicular to the Z disks arrows in upper panel, (Figure 3C). Only few intermyofibrillar mitochondria remained arrow lower panel, (Figure 3C). Moreover, mitochondria localized in the subsarcolemmal space seemed more densely packed and swollen in RAmKO mice (Figure S4A). As a decrease in oxidative properties is often accompanied by a compensatory increase in glycolytic activity, we performed a periodic acid Schiff (PAS) staining. Indeed, the glycogen content was increased in both EDL and soleus muscle (Figure 3D). The increase was more pronounced in the fast-twitch EDL muscle. The glycogen content in the gastrocnemius muscle, which consists of a mixed population of fast- and slow-twitch fibers, was more than 5 times higher than in control mice (control: 21 ± 7 μ mol glucose/g tissue; RAmKO: 108 ± 22 μ mol glucose/g tissue; mean \pm SEM; N = 4 mice). The change in oxidative capacity and glycogen content in skeletal muscle also affected overall metabolism as glucose uptake from the blood was significantly slower in RAmKO mice compared to littermate controls (Figure 3E).

High content of glycogen is indicative of fast-twitch type II muscle fibers. To test whether muscles in RAmKO mice also changed their structural properties, we stained EDL and soleus muscle for the slow myosin heavy chain (sIMHC), a marker of slow-twitch fibers. Surprisingly, EDL and soleus muscle of 140 day-old RAmKO mice contained even more sIMHC-positive muscle fibers (Figure 3F); green than controls and the increase of sIMHC was regionalized in individual muscles (Figure S4B). In both muscles, the number of sIMHC-positive fibers was approximately 2 to 3 times higher than in controls (Figure 3G & H). In soleus muscle of RAmKO mice, almost 100% of the fibers were positive for sIMHC (Figure 3H) and this increase was also seen by Western blot analysis (Figure 3I; Table S1). Moreover, other components characteristic for slow-twitch muscle, such as the slow isoform of troponinT (sITnT) and of troponinI (sITnI), were also increased in soleus muscle of RAmKO mice (Figure 3I & J; Table S1). Thus, deletion of mTORC1 in skeletal muscle fibers causes a shift of their metabolic properties from oxidative to glycolytic. However, this change in the metabolic characteristics of muscles is opposite to their structural properties.

3.4. Functional characterization of muscles in RAmKO mice

To address whether the observed changes in metabolic and structural characteristics had consequences on the overall performance of muscle, we allowed 90 day-old mice to exercise using voluntary wheel running. The representative activity chart of a single mouse shows that running sessions of RAmKO mice were shorter and less frequent than those of controls (Figure 4A). When averaged over one week, the total distance run per day by RAmKO mice was ~ 60% of that of control mice (Figure 4B) and the top running speed was significantly lower (Figure 4C). In contrast to the aerobic wheel running task, RAmKO mice performed equally well as control animals in a grip strength test on a horizontal grid (Figure 4D). To examine the contraction properties of muscles, force measurements were performed on isolated EDL and soleus muscles. In line with the observed increase of fibers expressing structural proteins characteristic of slow-twitch muscle, time to peak, half time to peak and relaxation time of the twitch were all increased (Table 2). This difference to control mice did not reach significance in EDL muscle but was highly significant in soleus muscle (Table 2). Twitch force and maximal tetanic absolute force for both muscles was, however, significantly lower in RAmKO mice. The decrease of absolute force capacity reflects the decrease of muscle mass (Table 1), since there is no difference of the maximal tetanic force when normalized to the muscle cross-sectional area (Table 2). An intermittent maximal tetanic stimulation protocol revealed that both EDL and soleus muscle from RAmKO mice were more resistant to fatigue (Figure 4E). These data indicate that raptor-deficient muscle fibers have a reduced aerobic capacity voluntary wheel running like fast-twitch, glycolytic muscle fibers, but exert contraction properties isolated muscles of slow-twitch, oxidative muscle fibers.

3.5. Inactivation of raptor or rictor affects activation of PKB/AKT

In search of a mechanistic explanation for the phenotypes, we examined soleus muscle of RAmKO and RImKO mice biochemically. In each experiment, at least three different mice were compared with three littermate controls. Deletion of raptor or rictor did not significantly affect the levels of mTOR (Figure 5A, Table S1). The levels of rictor were not lowered in RAmKO mice and there was a slight decrease of raptor in RImKO mice (Figure 5A, Table S1). The amount of S6K, S6 and 4EBP1, which are the main targets of mTORC1, was not changed in RAmKO mice. However, phosphorylation of S6 and 4EBP1 was strongly decreased (Figure 5A; Table S1). In RImKO mice, mTORC1 targets were not changed but the level and activation state of PKB/AKT and PKC α , which are both well characterized substrates of mTORC2 [60, 71], were lower. More importantly, phosphorylation of PKB/AKT on residues Thr308 and Ser473 was strongly increased in RAmKO mice (Figure 5A; Table S1). Furthermore, the total amount of FOXO1 and FOXO3a was increased in RAmKO mice concomitant with an increase in phosphorylation of FOXO1 on Thr24 (Figure 5A; Table S1). In contrast, phosphorylation of FOXO1 on Ser316 and of FOXO3a on Thr32 was not increased.

Activation of S6K by mTORC1 causes feedback inhibition of the insulin/IGF-1 pathway by affecting the levels and the phosphorylation of IRS-1 [119, 134]. Consistent with this notion, deficiency of mTORC1 and thus absence of S6K/S6 activation abrogated this inhibitory feedback and strongly increased IRS-1 levels in muscles of RAMKO mice (Figure 5B; Table S1). Concomitant with the high protein levels, IRS phosphorylation on Ser636 and Ser639 was increased. On the other hand, both the levels and phosphorylation of the mitogen-activated protein kinase ERK1 and ERK2 were not significantly changed (Figure 5B; Table S1). Thus, activation of PKB/AKT is probably due to the failure of raptor-deficient muscle fibers to activate S6K and thus due to the absence of the inhibitory feedback onto IRS. The release of this feedback in muscle may require prolonged inactivation of mTORC1 as phosphorylation of PKB/AKT was not increased after 8 hour treatment of cultured C2C12 myotubes with rapamycin and was only slightly elevated after 16 hours (Figure S5C).

Next we asked whether part of the phenotype of RAMKO mice could be based on this hyperphosphorylation of PKB/AKT. To determine whether PKB/AKT was indeed activated within muscle fibers and not in non-muscle tissue of RAMKO mice; we stained cross-sections of soleus muscle with antibodies specific for PKB/AKT phosphorylated on Ser473 (P-PKB/AKTS473). Indeed, many of the muscle fibers were strongly positive for P-PKB/AKTS473 (Figure S5A). PKB/AKT has been shown to regulate expression of atrogenes, called atrogen-1/MAFbx and MuRF-1, via FOXO [151, 152]. As expected, mRNA levels for both atrogenes were significantly lower in RAMKO mice than in controls (Figure 5C). A further target of PKB/AKT is GSK3 β , which in turn inhibits glycogen synthase [153]. Whereas the amount of GSK3 β was unaffected, phosphorylation of Ser9 was significantly increased (Figure 5C; Table S1). Moreover, glycogen phosphorylase, which is the enzyme that generates free glucose from glycogen, was downregulated (Figure 5C; Table S1). Thus, hyperphosphorylation of PKB/AKT in conjunction with downregulation of glycogen phosphorylase is probably the basis for the increased levels of glycogen observed in RAMKO mice.

In an attempt to identify the pathway that might underlie the increased number of muscle fibers expressing sIMHC, we found a slight increase in the levels of calcineurin and a highly significant increase in myocyte-enhancer factor 2A (Mef2A); (Figure 5C; Table S1). A slight, but not significant increase in Mef2D was also observed. The increase in Mef2A is not a consequence of the ongoing de- and regeneration in soleus muscle as Mef2A was also increased in the least affected EDL muscle (Figure S5B). In contrast to skeletal muscle in vivo, Mef2A and sIMHC were not increased in cultured C2C12 myotubes upon prolonged treatment with rapamycin (Figure S5C).

3.6. Genes involved in mitochondrial biogenesis are downregulated in RAMKO mice

One of the most striking features of RAMKO skeletal muscle is its lower oxidative capacity that is probably due to ultrastructural changes and loss of mitochondria. Thus, we also tested whether genes involved in mitochondrial biogenesis were affected by the deletion of raptor. Recent evidence indicates a function of mTORC1 in the regulation of mitochondrial function via PGC1 α [40]. Consistent with these findings, transcript levels for PGC1 α and for its target gene myoglobin were significantly reduced

in RAmKO muscle (Figure 5E). Moreover, the protein levels of the PGC1 α co-activator PPAR γ and the mitochondrial marker cytochrome c oxidase IV (COX IV) were significantly decreased in RAmKO mice (Figure 5F; Table S1). These results are consistent with the low oxidative capacity of muscle from RAmKO mice and they support the notion that this is due to loss of PGC1 α .

3.7. Activation of PKB/AKT is independent of mTORC2

To test whether the hyperactivated state of PKB/AKT in RAmKO mice can be prevented by additional deletion of rictor, we generated double floxed mice and mated those with HSA-Cre mice. The resulting mice, called DmKO, lacked both raptor and rictor in skeletal muscle (Figure 5G; Table S1). Their overall phenotype was indistinguishable from RAmKO mice data not shown. Like in RAmKO mice, skeletal muscle of DmKO mice contained high levels of glycogen and was less oxidative (Figure 5H). Levels of mTOR were significantly lower in DmKO mice than in either of the single knockouts (Figure 5G; Table S1). As mTORC2 was shown to phosphorylate PKB/AKT on Ser473 [71], we also tested the activation state of PKB/AKT in DmKO muscle. As shown in Figure 5G and in Table S1, PKB/AKT was still hyperphosphorylated on Thr308 and Ser473 in DmKO mice. Again, phosphorylation of PBK/Akt occurred only in muscle fibers and not in non-muscle tissue (Figure 5J). In summary, these results indicate that mTORC2 is not the only kinase that phosphorylates PKB/AKT on Ser473.

4. DISCUSSION

Our work dissects the role of raptor and rictor i.e. mTORC1 and mTORC2, respectively in skeletal muscle. The HSA-Cre mice used for our experiments start to express Cre at the earliest stages of skeletal muscle development when the first myotubes are formed. In fully developed muscle, Cre is exclusively expressed in skeletal muscle fibers but not in non-muscle cells, such as Schwann cells, fibroblasts or satellite cells [143]. Neither RAmKO nor RimKO mice showed any abnormalities at birth, indicating that mTORC1 and mTORC2 are not essential for muscle development. Whereas no overt phenotype was detected in RimKO mice throughout adulthood, which is consistent with another report [154], RAmKO mice developed a progressive dystrophy and ultimately died around the age of five months. Interestingly, DmKO mice showed very similar pathological changes as RAmKO mice, indicating that mTOR function in skeletal muscle requires only mTORC1.

The dystrophy in RAmKO mice did not affect all muscles to the same extent. For example, diaphragm and soleus muscles were severely affected while EDL showed much less changes. Prominent features of the dystrophy were elevated numbers of muscle fibers with centralized nuclei and the presence of central core-like structures. Central cores are hallmarks of “central core diseases”, which are inherited neuromuscular disorders with a myopathic syndrome. The most frequent causes of this group of diseases are mutations in the ryanodine receptor, which is the main protein responsible for calcium homeostasis in muscle reviewed in [155]. Thus, the similarity of the pathology in RAmKO to this class of disease suggests that mishandling of intracellular calcium may underlie the disease. The low levels of PGC1 α may additionally contribute to the dystrophic phenotype of RAmKO mice as conditional ablation of PGC1 α in skeletal muscle results in a myopathic phenotype [156]. Finally, several metabolic diseases that cause accumulation of glycogen in skeletal muscle, such as Pompe’s and McArdle’s disease, affect skeletal muscle function. The most severely affected patients may even die because of respiratory distress [157]. In summary, RAmKO show changes in muscle homeostasis that together may lead to the progressive muscle dystrophy.

4.1. Raptor is required for high oxidative capacity of skeletal muscle

We found that the severity of the muscle dystrophy correlated with the relative levels of raptor, rictor, mTOR and PKB/AKT in particular muscles. Interestingly, the most affected muscles, such as soleus or diaphragm, are also those that are insulin-sensitive [158] and contain a high number of slow-twitch, oxidative fibers. Biochemical and morphological analysis showed that soleus muscle expressed little of the oxygen carrier myoglobin and of COXIV, and contained fewer and misshaped mitochondria. A direct role of mTOR and raptor for the function of mitochondria has recently been suggested using cultured Jurkat cells [39]. Moreover, mTOR has been shown to form a complex with PGC1 α [40], which together with its cofactor PPAR γ is a key regulator of mitochondrial biogenesis and function. Consistent with a regulatory function of mTORC1 for mitochondria, mRNA levels for PGC1 α and

protein levels of PPAR γ were decreased in RAmKO mice. Furthermore, mRNA and protein levels of target genes for PGC1 α /PPAR γ , such as myoglobin [58] and glycogen phosphorylase [159] were also reduced in RAmKO mice. Also, very similar to the phenotype of RAmKO mice, a reduced intermyofibrillar mitochondrial content in slow-twitch muscles has been reported in PGC1 α knockout mice [160]. In summary, our data indicate that mTORC1 is essential for the function of mitochondria in skeletal muscle and they link mTORC1 to the regulation of PGC1 α in vivo.

4.2. Segregation of metabolic and structural properties in skeletal muscle of RAmKO mice

Despite the loss of oxidative capacity and the downregulation of PGC1 α , expression of slow structural proteins (sISP); (Figure 5K) was increased in RAmKO mice. Analysis of the mechanical properties in EDL and soleus muscle further confirmed that both muscles adapt characteristics indicative of slow-twitch fibers. These results suggest that RAmKO mice induce a structural program for slow-twitch fibers. As muscle-specific inactivation of PGC1 α causes a fiber-type switch to fast-contracting muscle fibers [161] and transgenic overexpression causes an increase in oxidative muscle [58], we also tested whether any other pathways that affect muscle differentiation were altered in the RAmKO mice. Besides PGC1 α , the best characterized factors involved in fiber type determination are calcineurin/NFAT and the Mef2 transcription factors [162]. Of those candidate genes, the levels of calcineurin and in particular of Mef2A and Mef2D were increased in RAmKO mice. Thus, facilitated Mef2-mediated transcription may be the basis for the increased levels of sISP despite the low levels of PGC1 α . Opposite regulation of PGC1 α and Mef2A has also been seen in cultured cells when treated with rapamycin [40]. Mef2 has also been shown to be dominant in the regulation of muscle fiber type as transgenic overexpression of a constitutively active form of Mef2 is sufficient to increase the number of slow muscle fibers [163]. Mef2 is generally thought to be controlled by calcium-activated processes acting via calcineurin and CaM kinase IV [164]. In this context it is interesting to note that the increase of the half-relaxation time in RAmKO muscles may result from a lower removal rate of calcium from the myoplasm by the sarcoplasmic reticulum [165]. This prolonged presence of intracellular calcium during contractile activity might contribute to the activation of calcium-dependent signaling pathways, and thus to the upregulation of sISP (Figure 5K). On the other hand, it is possible that Mef2 expression is increased because of hyperactivation of PKB/AKT [166]. Consistent with this notion, failure to induce a pronounced phosphorylation of PKB/AKT in cultured C2C12 myotubes by treatment with rapamycin coincided with unchanged levels of Mef2A and sIMHC (Figure S5C).

4.3. Raptor deficiency affects protein synthesis directly and PKB/AKT activation indirectly

Ablation of mTORC1 in skeletal muscles prevented phosphorylation of S6K/S6 and 4EBP1. This branch of the mTOR signaling pathway is characterized best and has been shown to directly control protein synthesis. Impaired efficacy of protein synthesis in postnatal muscle might also be the reason for the muscles being lighter in RAmKO mice. This effect may also contribute to the shift in fiber size distribution towards smaller values. Our data thus implicate mTORC1 in the maintenance of mass

even in fully innervated muscle. Therefore, they extend previous results in which mTOR inhibition by rapamycin was shown to prevent compensatory hypertrophy and recovery from atrophy but not cause atrophy [8]. Our results are also consistent with the findings that skeletal muscles of S6K-deficient mice are atrophic [9]. The difference in weight of the RAmKO mice became significant only after the age of approximately 2 months, suggesting that the absence of raptor might be compensated for during early periods of muscle growth. One compensatory mechanism could be PKB/AKT-mediated phosphorylation of GSK3 β as inhibition of GSK3 β has been shown to cause hypertrophy in cultured C2C12 myotubes [50]. We also provide evidence that the lack of S6K activation in RAmKO mice is responsible for the hyperphosphorylation of PKB/AKT on Thr308 and Ser473 as levels of IRS-1 were highly increased. Activation of S6K has been shown to decrease the levels of IRS-1 reviewed in [167]. Interestingly, the same hyperactivation of PKB/AKT is seen in mice with an adipocyte-specific ablation of raptor [144].

4.4. Raptor-deficient skeletal muscles are small, despite high energy consumption

Whereas changes in mitochondrial content and function might be based on a direct influence of mTORC1 (Figure 5K), other aspects such as the loss of adipose tissue are probably a consequence of the hyperactivation of PKB/AKT. Muscle-specific overexpression of a constitutively active form of PKB/AKT causes pronounced hypertrophy [6]. Concomitantly with the hypertrophy, mice are lean and do not become obese on a high fat diet [6]. In the RAmKO mice, PKB/AKT was hyperactive resulting in mice that had much less fat than control mice on a normal chow diet Table 1 or on a high fat diet (KR, CFB and MAR), unpublished observation. In contrast to mice that express the constitutively active form of PKB/AKT, lack of mTORC1 prevented the "translation" of PKB/AKT activation into muscle hypertrophy in RAmKO mice. Thus, RAmKO mice behave metabolically like mice that overexpress activated PKB/AKT but lack the hypertrophic effect on muscle. We hypothesize that the metabolic phenotype of being lean is due to the high need of muscle for glucose because of their high glycogen storage capability and their low capacity for oxidative phosphorylation. If the muscle of RAmKO mice acts as such a global glucose sink, non-muscle tissues may have to use alternative energy sources such as fatty acids. This, in turn, could result in an increased release and mobilization of fatty acids from adipose tissue. The high content of glycogen is probably based on the hyperactivation of PKB/AKT, which inhibits GSK3 β , which in turn, releases inhibition of glycogen synthase (Figure 5H). In addition, inhibition of GSK3 β also lowers phosphorylation of NFATc and thus prolongs its activity in the nucleus [168]. NFATc transcription factors, which are also targets of calcineurin see above, are known to contribute to fiber type selection reviewed in [169]. Thus, changes in NFATc activity may add to the expression of structural proteins indicative of slow-twitch muscle.

4.5. Hyperactivation of PKB/AKT does not require rictor/mTORC2

Our data strongly indicate that the absence of the S6K-mediated inhibitory feedback caused phosphorylation of PKB/AKT on Thr308 and Ser473 in RAmKO mice. While phosphorylation on

Thr308 is mediated by 3-phosphoinositide-dependent kinase PDK1; [170], mTORC2 has been shown to phosphorylate PKB/AKT on Ser473 [71]. Consistent with such a role for mTORC2, we and others observed a decrease in Ser473 phosphorylation in mice deficient for rictor (Figure 5) [11, 12, 154]. We now show that unexpectedly, muscles from mice lacking both mTORC1 and mTORC2 still showed a marked increase in PKB/AKT phosphorylation on both Thr308 and Ser473. Thus, mTORC2 is not required to phosphorylate PKB/AKT on Ser473 in vivo, indicating that skeletal muscles express a PDK2 distinct from mTORC2. A candidate for this kinase is DNA-PK, which has been shown to phosphorylate PKB/AKT in cells that are deficient for rictor in response to DNA damage [79]. DNA-PK and PKB/AKT are localized in the nucleus of embryonic fibroblasts upon DNA damage [79]. However, PKB/AKT phosphorylated on Ser473 in DmKO mice was expressed along the sarcolemma and not specifically localized in myonuclei. Several additional proteins have been postulated to act as PDK2, some of which are expressed in skeletal muscle and are localized to the sarcolemma (see [171] for a review).

In summary, our data show that mTORC1 is important for the function and maintenance of skeletal muscle. We provide evidence that the different aspects of the phenotype observed in RAmKO mice are probably based either on the direct effect of mTORC1 on its downstream targets S6K and 4EBP1, on the function of mTORC1 to regulate mitochondrial biogenesis and function via PGC1 α , or on an indirect effect on its upstream component PKB/AKT. Our data also suggest that long-term treatment with high doses of rapamycin may have detrimental effects on muscle function.

5. EXPERIMENTAL PROCEDURES

Antibodies

Rabbit polyclonal antibodies: 4E-BP1 Phas-I from Zymed, ERK1&2 pan and ERK1&2 pTpY185/187 from Biosource, FOXO1a and FOXO1a phospho S319 from Abcam, P-PKC α Ser657 and Troponin T-SS H-55 from Santa Cruz, Phospho-4E-BP1 Ser65, PAN-actin, Akt, Phospho-Akt Thr308, Pan-Calcineurin A, Phospho-FOXO1 Thr24/ FOXO3a Thr32, Phospho-GSK-3 β Ser9, Phospho-IRS-1 S636/639, MEF2A, mTOR, PKC α , S6 Ribosomal Protein, Phospho-S6 Ribosomal Protein Ser235/236 and p70 S6 kinase from Cell Signaling. Rabbit monoclonal antibodies: β -actin, Phospho-Akt Ser473, Cox IV, FOXO3a 75D8, GSK-3 β , IRS-1, PI3 Kinase p85, Raptor and Rictor from Cell Signaling and PPAR γ from Santa Cruz. Mouse monoclonal antibodies: α -actinin and myosin skeletal, slow from sigma, β -tubulin and Mef2D from BD Biosciences. Goat polyclonal antibody: GP from Santa Cruz.

Tissue homogenization, immunoprecipitation, SDS PAGE and Western blot

Muscles frozen in liquid nitrogen were powdered on dry ice, transferred to cold RIPA buffer supplemented with 1% Triton-X, 10% glycerol, protease inhibitor cocktail tablets Roche and phosphatase inhibitor cocktail I and II Sigma. Cell lysates were incubated on ice for 2 hours, sonicated 2 times for 15 seconds and centrifuged at 13,600g for 30 min at 4°C. Cleared lysates were then used to determine total protein levels BCA Protein Assay, Pierce. After dilution with sample buffer, equal protein amounts were loaded onto SDS gels.

Histology and immunohistochemistry

Muscles frozen in liquid nitrogen-cooled isopentane were fixed with 2% PFA and cut into 12 μ m cross-sections. Cross-sections were permeabilized with 1% Triton/PBS for 5 min, washed with 100 mM glycine/PBS for 15 min, blocked with 1% BSA/PBS for 30 min and incubated with specific primary antibody overnight at 4°C. Samples were subsequently washed with 1% BSA/PBS, 3 times for 1 hour, stained with appropriate fluorescently labeled secondary antibodies for 1 hour at room temperature. After washing with PBS, samples were mounted with Citifluor Citifluor Ltd. General histology on cross-sections was performed using hematoxylin and eosin H&E; Merck, Rayway, NJ, USA. NADH staining was done as described [172]. Periodic acid-schiff staining PAS staining system, Sigma was performed according to the manufacturer's instruction. After H&E, NADH and PAS staining, samples were dehydrated and mounted with DePeX mounting medium Gurr, BDH.

Mice

PAC clones from the RPCI-21 129S6 mouse genomic DNA library [173] were identified by hybridization with cDNA encoding the targeted exons. For raptor, a 6.9 kb SmaI fragment spanning 2.9

kb upstream and 3.8 kb downstream of raptor exon 6 was isolated from clone RPCI-21 388E14 and cloned into pBluescript Stratagene. For the rictor targeting construct, a 10.3 kb EcoRI fragment that encompassed 4.5 kb upstream of exon 4 and 4.5 kb downstream of exon 5 was isolated from clone RPCI-21 520C16 and ligated into pBluescript. Using homologous recombination ET cloning as well as Cre-driven recombination in bacteria and standard cloning procedures, recombination sites, a selection cassette and diagnostic restriction sites were added to the vectors. The neomycin resistance PGK-TK-neo cassette flanked by two Frt recombination sites and a 5'-LoxP site was added 283 bp upstream of exon 6 in the raptor construct and 304 bp upstream of exon 4 in the rictor construct [174]. The 3'-LoxP sites were located 277 bp downstream of raptor exon 6 and 301 bp downstream of rictor exon 5, respectively. The targeting vectors were linearized and electroporated into R1 ES cells derived from 129S6 mice [175]. Clones were analyzed for correct integration by Southern blot analysis using both 5'- and 3'-probes (see Figures 1A and B). Chimeric mice were obtained by microinjection of the correctly targeted clones into C57BL/6 blastocysts. Chimeric mice were crossed with C57BL/6 mice to obtain germline transmission. Mice analyzed in this study were backcrossed to C57BL/6 for 4 generations. The backcrosses involved mice constitutively expressing the FLP recombinase to excise the neomycin cassette from the targeted allele [142] and mice expressing the Cre recombinase under the human skeletal actin promoter [143]. As indicated in Figure 1, PCR genotyping of RAmKO mice was performed with primers P1: 5' ATG GTA GCA GGC ACA CTC TTC ATG and P2: 5' GCT AAA CAT TCA GTC CCT AAT C, resulting in an amplicon of 228 bp in case of presence of the FRT site and of 141 bp in case of the wild-type allele. For RImKO mice, primers P1: 5' TTA TTA ACT GTG TGT GGG TTG and P2: 5' CGT CTT AGT GTT GCT GTC TAG, resulting in an amplicon of 295 bp in case of presence of the FRT site and of 197 bp in case of a wild-type allele were used. The monoallelic presence of the Cre recombinase was detected using primers F: 5' TGT GGC TGA TGA TCC GAA TA and B: 5' GCT TGC ATG ATC TCC GGT AT resulting in an amplicon of 249 bp. Tissue-specific LoxP recombination in RAmKO mice was determined with primers P1 and P3: 5' CTC AGA GAA CTG CAG TGC TGA AGG, resulting in an amplicon of 204 bp for the recombined allele and no product for the wild-type or unrecombined allele (Figure 1C). LoxP recombination in RImKO mice was detected using primers P1 and P3: 5' CAG ATT CAA GCA TGT CCT AAG C resulting in a PCR product of 280 bp in presence of the recombined allele and in no product in wild-type or unrecombined allele. DmKO mice were genotyped with the primers used for RAmKO and RImKO mice. Brain-specific raptor and rictor knockout mice were obtained by crossing floxed mice with Nestin-Cre mice [176]. Mdx mice were obtained from the Jackson Laboratory.

Animal care, body weight, food intake and body temperature measurements

Mice were maintained in a conventional facility with a fixed light cycle. Studies were carried out according to criteria outlined for the care and use of laboratory animals and with approval of the Swiss authorities. Body weight, food intake and body temperature were measured weekly. A medical precision thermometer DM 852 from Ellab was used for the body temperature measurements.

Real-time PCR

Total RNA was isolated SV Total RNA isolation System, Promega from soleus muscles. Reverse transcription was carried out using a mixture of oligodT and random hexamer primers iScript cDNA Synthesis Kit, Bio-Rad. Sybr Green, real-time PCR analysis Power SYBR Green Master Mix, Applied Biosystems was performed using the ABI Prism 7000 Sequence Detector. Expression levels for each gene of interest were normalized to the mean cycle number using real-time PCR for the two housekeeping genes β -actin and Polr2A. In all experiments, the ratio between β -actin and Polr2A was constant. The following primers were used: β -actin sense primer: 5' CAG CTT CTT TGC AGC TCC TT, antisense primer: 5' GCA GCG ATA TCG TCA TCC A; Polr2A sense primer: 5' AAT CCG CAT CAT GAA CAG TG, antisense primer: 5' CAG CAT GTT GGA CTC AAT GC; MAFbx sense primer: 5' CTC TGT ACC ATG CCG TTC CT, antisense primer: 5' GGC TGC TGA ACA GAT TCT CC; MuRF1 sense primer: 5' ACG AGA AGA AGA GCG AGC TG, antisense primer: 5' CTT GGC ACT TGA GAG GAA GG; sTnl sense primer: 5' GTG CCT GGA ACA TCC CTA AT, antisense primer: 5' TGA GAG GCT GTT CTC TCT GC; PGC1 α sense primer: 5' AAC GAT GAC CCT CCT CAC AC, antisense primer: 5' TCT GGG GTC AGA GGA AGA GA; myoglobin sense primer: 5' ATC CAG CCT CTA GCC CAA TC, antisense primer: 5' GAG CAT CTG CTC CAA AGT CC.

In vitro muscle strength assessment

EDL and soleus muscles were dissected and mounted into a muscle testing setup Heidelberg Scientific Instruments. Muscle force assessment was carried out as previously described [177]

Voluntary wheel running

Animals were individually housed in cages equipped with a running wheel carrying a magnet. Wheel revolutions were registered by a reed sensor connected to an I-7053D Digital-Input module Spectra, and the revolution counters were read by a standard laptop computer via an I-7520 RS-485-to-RS-232 interface converter Spectra. Digitalized signals were processed by the "mouse running" software developed by Santhera Pharmaceuticals.

Assessment of muscle fiber membrane damage

Mice were forced to run downhill on a treadmill with an inclination of 15°, at the speed of 10 m/min for 10 min. This procedure was repeated for 3 days. After the second running session, Evans blue dye 1 mg / 0.1 ml PBS / 10 g body weight was injected intraperitoneally. Mice were sacrificed 1 hour after the last running session and cross-sections of the entire hindleg were analyzed [178].

Glucose tolerance test

60 to 65 day-old mice were fasted overnight, followed by an intraperitoneal injection of 2 g/kg glucose. Blood was obtained from the tail vein at the indicated time points and analyzed using a OneTouch UltraMini Meter Lifescan.

Electron microscopy

Transmission electron microscopy was performed as described [179].

Tissue culture

C2C12 cells were differentiated using DMEM containing 5% horse serum for 72 h before treatments with vehicle or rapamycin 8 or 16 h at 20 nM.

Heart weight and function

Under isoflurane anaesthesia, parasternal short axis M- and B-mode images of the left ventricle were obtained using a VisualSonics 770 machine with a 40-MHz linear transducer. Heart rate HR, left ventricular end-diastolic diameter LVEDD, left ventricular end-systolic diameter LVESD, diastolic and systolic posterior wall and septum thickness were determined. Fractional shortening %FS was calculated as $LVEDD - LVESD / EDD \times 100$. Left ventricular weight was calculated from the cardiac dimensions obtained by the VisualSonics system and confirmed by directly weighing the wet hearts after sacrifice of the mice.

Quantifications and statistics

Muscle glycogen concentration was measured in homogenates after 2 h of hydrolysis in 2N HCl at 100°C. The resulting free glucosyl units were determined using a commercial hexokinase-based assay kit Sigma. For muscle fiber size quantification, pictures were collected using a Leica DM5000B fluorescence microscope, a digital camera F-View; Soft Imaging, and analySIS software Soft Imaging System. Muscle fiber size distribution was determined on laminin- γ 1 immunostained muscle cross-sections using the minimum distance of parallel tangents at opposing particle borders minimal "Feret's diameter" as described elsewhere [180]. Quantification of Western blots was performed using the ImageJ software. Background-corrected grey values were normalized to total protein levels. Compiled data are expressed as mean \pm SEM. For statistical comparisons of two conditions, the Student's t- test was used. The level of significance is indicated as follows: *** $p < 0.001$, ** $p < 0.01$, * $p < 0.05$.

6. TABLES

Table 1	90d		140d	
	ctrl	RAmKO	ctrl	RAmKO
Tibia length cm	2.0 ± 0.1	2.0 ± 0.1	2.0 ± 0.1	2.1 ± 0.1
Lower hindleg mg	449.2 ± 19.3	344.0 ± 11.4***	428.0 ± 28.0	331.6 ± 41.3**
Triceps brachii mg	98.3 ± 11.3	67.0 ± 10.4***	89.5 ± 14.0	68.8 ± 13.8*
Soleus mg	9.7 ± 0.8	7.4 ± 0.6***	9.2 ± 0.8	7.1 ± 1.2*
EDL mg	12.7 ± 0.8	10.3 ± 0.7***	12.0 ± 0.7	9.4 ± 1.4*
Tibialis anterior mg	58.3 ± 2.7	40.8 ± 2.3***	55.6 ± 1.8	39.0 ± 1.3***
Epididymal fat pad mg	566.4 ± 214.9	438.9 ± 93.1	616.0 ± 194.8	242.5 ± 118.7**
Heart mg	85.12 ± 6.6	68.1 ± 4.1*	88.5 ± 2.1	72.1 ± 4.4**
Liver mg	1350.9 ± 185.0	1187.5 ± 161.0	1232.0 ± 187.5	1055.0 ± 269.1

* p<0.05, ** p<0.01, ***p<0.001

Table 1. Analysis of particular tissues in control and RAmKO mice. Weight or length was measured for different muscles, bones and other organs in 90- and 140 day-old mice. P-values determined by Student's t-test are indicated by asterisks N = 4 mice. Values represent mean ± SD.

Table 2	EDL		Sol	
	ctrl	RAmKO	ctrl	RAmKO
Twitch				
Time to peak ms	10.1 ± 0.9	11.1 ± 1.2	20.3 ± 4.2	39.7 ± 2.4***
Half time to peak ms	3.0 ± 0.4	3.5 ± 0.5	5.6 ± 0.6	11.6 ± 1.1***
Half relaxation time ms	15.5 ± 2.2	16.8 ± 3.3	30.8 ± 8.7	63.0 ± 5.1***
Absolute force mN	54.0 ± 13.2	45.0 ± 9.7	30.0 ± 5.6	21.0 ± 8.1*
Tetanus				
Half contraction time ms	16.6 ± 2.0	14.4 ± 1.1*	27.5 ± 5.4	41.0 ± 5.4***
Half relaxation time ms	22.1 ± 1.3	24.1 ± 1.6*	55.2 ± 3.9	124.4 ± 13.2***
Absolute force mN	311 ± 57.6	224 ± 38.1**	205 ± 20.8	164.0 ± 42.83
Specific force mN/mm ²	380.2 ± 57.2	328.3 ± 62.7	311.6 ± 56.3	264 ± 66.9

* p<0.05, ** p<0.01, ***p<0.001

Table 2. Analysis of the contractile properties of EDL and soleus muscles of control and RAmKO mice. Data were recorded from EDL and soleus muscles of 140 day-old mice. P-values determined by Student's t-test are indicated by asterisks N = 3 for RAmKO and N = 4 for control mice. Values represent mean ± SD.

7. FIGURES AND FIGURE LEGENDS

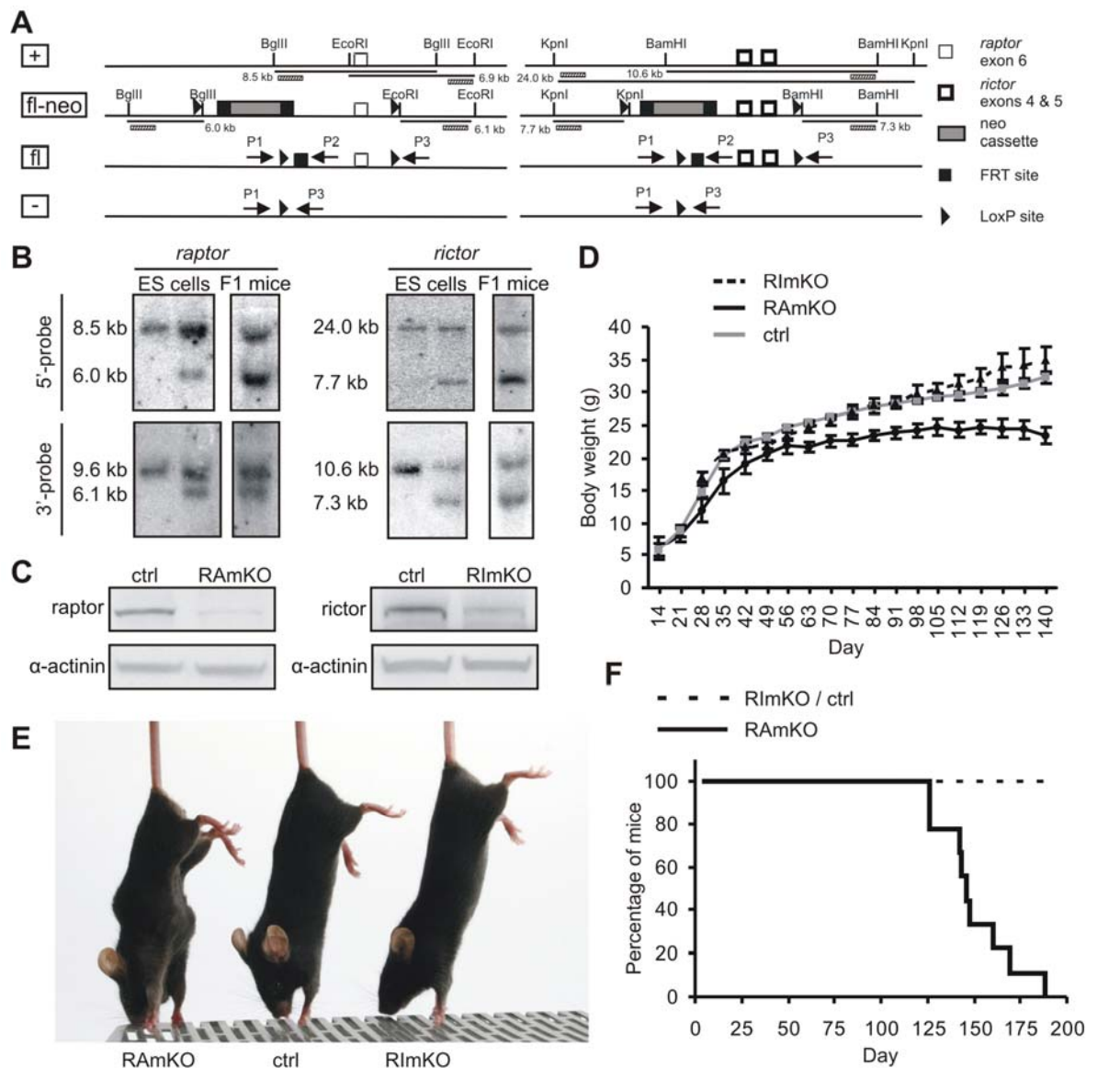


Figure 1. Targeting strategy and initial characterization of RAMKO and RImKO mice

(A) Schematic presentation of wild-type and targeted alleles of *raptor* left panel and *rictor* right panel before and after recombination. Localization and size of DNA fragments generated by particular restriction digests are indicated. Probes used for Southern blot analysis are shown by hatched bars. PCR primers for genotyping are indicated by arrows. +: wild-type allele; fl-neo: targeted allele; fl: alleles after recombination by FRT; -: alleles after recombination by Cre.

(B) Southern blot analysis of genomic DNA from ES cells and F1 progeny of resulting chimeras. Correct targeting of the 5' end is indicated by the presence of a 6.0 kb band in the *raptor* locus and a 7.3 kb band in the *rictor* locus. Correct targeting at the 3' end is indicated by a 6.1 kb and a 7.3 kb band, respectively. In each blot of ES cells, wild-type is to the left.

(C) Western blot analysis of protein extracts from skeletal muscle of RAmKO and RImKO mice. Controls correspond to muscle extracts from mice that carry the floxed alleles but are negative for HSA-Cre. Equal protein loading is confirmed by blotting for α -actinin.

(D) Growth curve of RAmKO, RImKO and control mice. Mice of each genotype were weighed every week. A significant difference between RAmKO and control mice $p < 0.05$ was observed after the age of 63 days. Individual data points represent means \pm SEM N = 5 for RAmKO; N = 3 for RImKO; N = 10 for controls.

(E) Photograph of 140 day-old RAmKO, control ctrl and RImKO mice.

(F) Survival curve of RAmKO , RImKO and control mice.

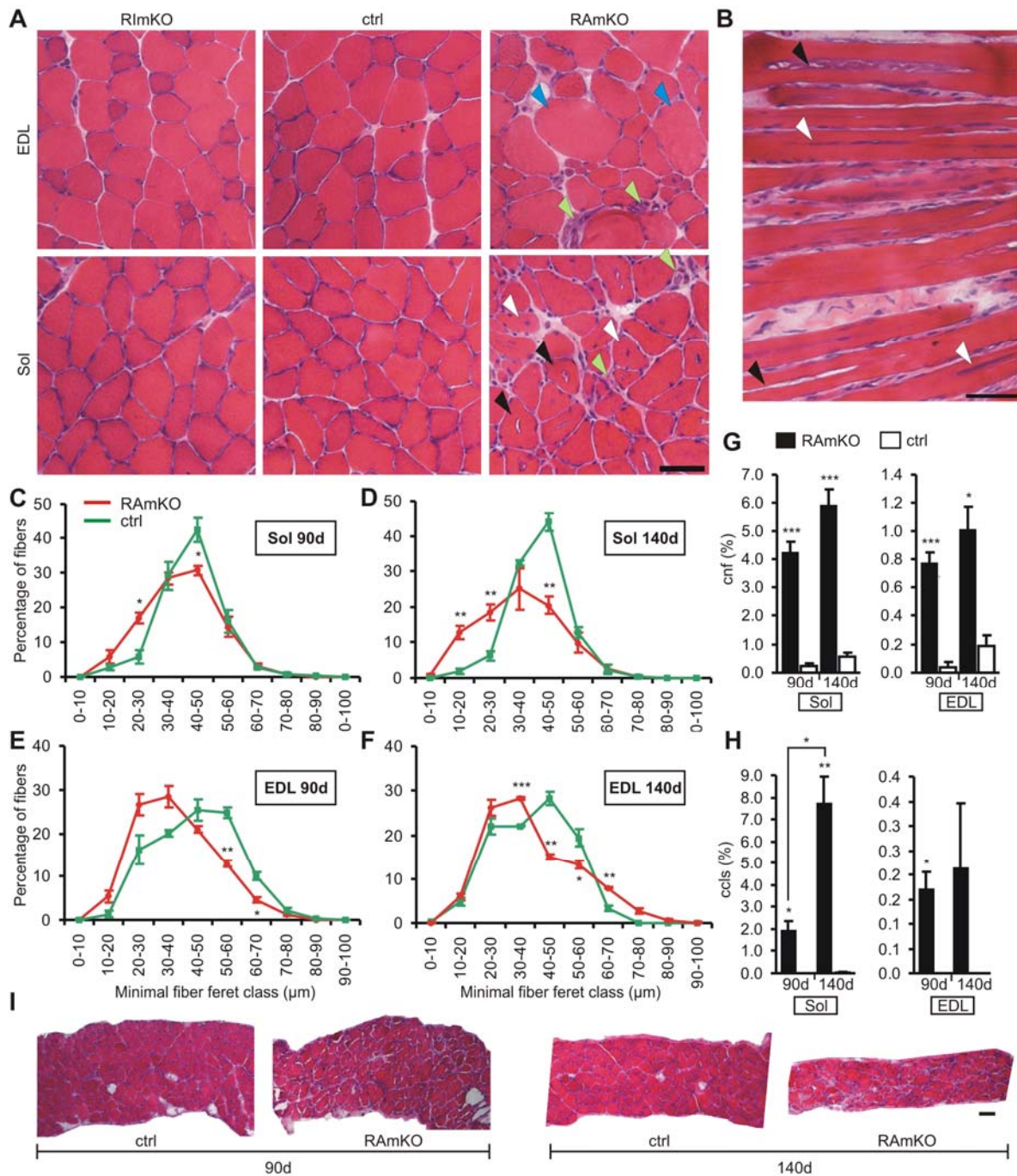


Figure 2. Muscle of RAmKO mice show signs of a progressive dystrophy

(A) Hematoxylin & Eosin H&E staining of muscle cross-sections from the EDL and soleus Sol muscle of 140 day-old mice. In EDL muscle of RAmKO mice, some large blue arrowheads but also small fibers are present. Centralized nuclei white arrowheads and central core-like structures black arrowheads can be found in soleus muscle of RAmKO mice. Both muscles contain many mononuclear cells green arrowheads.

(B) Longitudinal section of soleus muscle of a 140 day-old RAmKO mouse. Besides centrally aligned nuclei white arrowheads, central core-like structures black arrowheads, which expand longitudinally in muscle fibers are visible.

(C, D, E, F) Fiber size distribution in the soleus muscle of 90 day- C and 140 day-old D, and in the EDL muscle of 90 day- E and 140 day-old F RAmKO and control mice.

(G) Mean percentage of muscle fibers with centralized nuclei cnf in the soleus and EDL muscle of RAmKO and control mice.

(H) Percentage of muscle fibers containing central core-like structures ccls in soleus and EDL muscle of RAmKO and control mice.

(I) H&E staining of cross-sections of the diaphragm of 90 day- and 140 day-old RAmKO and control mice. Individual data points and bars C – H represent mean \pm SEM N=4 mice. Scale bars A, B, I = 50 μ m. P-values are: *** $p < 0.001$; ** $p < 0.01$; * $p < 0.05$.

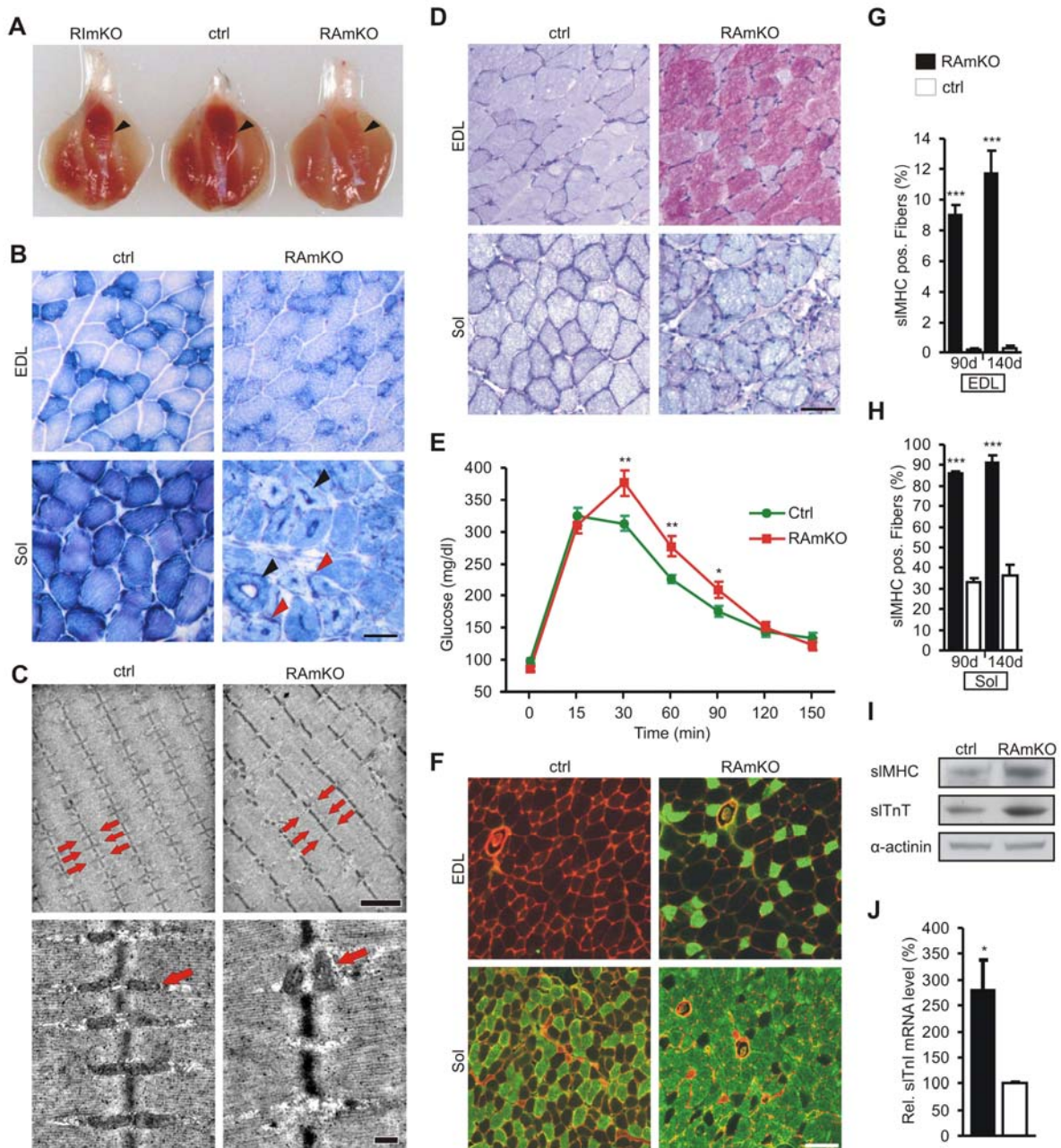


Figure 3. Metabolic and structural properties diverge in skeletal muscle of RAMKO mice

(A) Preparation of the entire hindleg isolated from 90 day-old mice of the genotypes indicated. Note that soleus muscle arrowheads is pale in RAMKO mice compared to RImKO and control mice.

(B) Activity of oxidative enzymes examined by NADH-tetrazolium staining blue precipitate in EDL and soleus muscle of 140 day-old mice. Central core-like structures devoid of NADH staining black arrowheads and increased subsarcolemmal reactivity red arrowheads was detected in some RAMKO soleus fibers.

(C) Electron micrographs of longitudinal sections of soleus muscle from 140 day-old mice. Most intermyofibrillar mitochondria in RAMKO muscle are lost from their specific position next to Z disks red

arrows, upper panel. Remaining mitochondria in RAmKO mice show high morphologic variability red arrow, lower panel.

(D) Periodic acid-schiff PAS staining of cross-sections from 140 day-old mice. The reaction product magenta color is indicative of the amount of glycogen in the tissue.

(E) Glucose tolerance test with 65 day-old mice N=8 for RAmKO and N=11 for control mice.

(F) Immunostaining for slow myosin heavy chain sIMHC; green and the laminin γ 1 chain red of cross-section from 140 day-old mice.

(G & H) Quantification of sIMHC-positive muscle fibers in soleus and EDL muscle from 90- and 140 day-old mice N = 4.

(I) Western blot analysis for sIMHC and slow troponin T sITnT using soleus muscle of 90 day-old mice. α -actinin is shown as a loading control.

(J) Relative mRNA levels of the slow skeletal muscle troponin I isoform sITnI in the soleus of 90 day-old mice as determined by QRT-PCR N = 3. Individual data points and bars E, G, H, J represent mean \pm SEM. Scale bars = 50 μ m B, D, 2 μ m upper pictures C, 250 nm lower pictures C and 125 μ m F. P-values are: *** p< 0.001; ** p< 0.01; * p< 0.05.

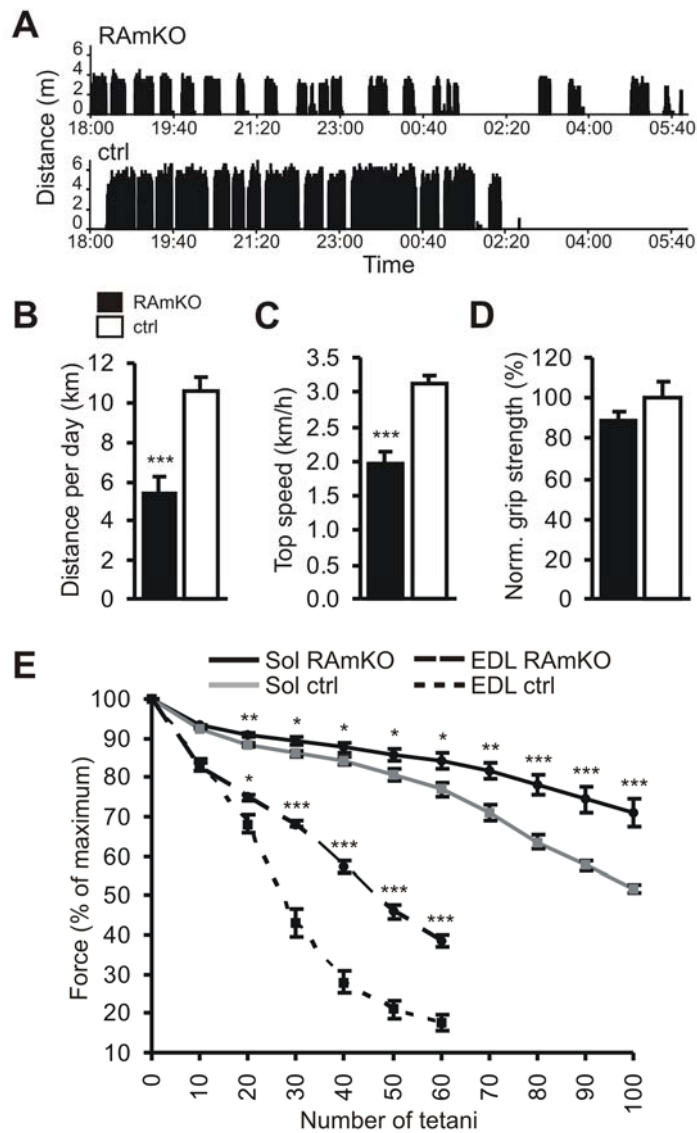


Figure 4. Exercise performance and muscle physiology

(A) Representative, activity chart with bins of 10 seconds from a single 95 day-old RAmKO or a control mouse. Charts were measured from 6 pm to 6 am dark cycle.

(B) Average distance run per day determined during one week starting at the age of 90 days, N = 4 for RAmKO and N = 9 for controls.

(C) Average of the top 10% speed measured over one week starting at the age of 90 days, N = 4 for RAmKO and N = 9 for controls.

(D) Grip strength of 90 day-old RAmKO and control mice. Average time mice were able to hold on a horizontal grid was normalized to body weight. Values of control mice were set to 100% N = 3.

(E) Force capacity resistance of EDL or soleus muscle isolated from 140 day-old mice was measured during muscle fatigue induced by intermittent tetanic stimulation. Trains of 150 Hz tetani of 350 ms duration were given at 3.6 s intervals. N = 3 for RAmKO and N = 4 for control mice. Individual data points and bars B – E represent mean \pm SEM. P-values are: *** $p < 0.001$; ** $p < 0.01$; * $p < 0.05$.

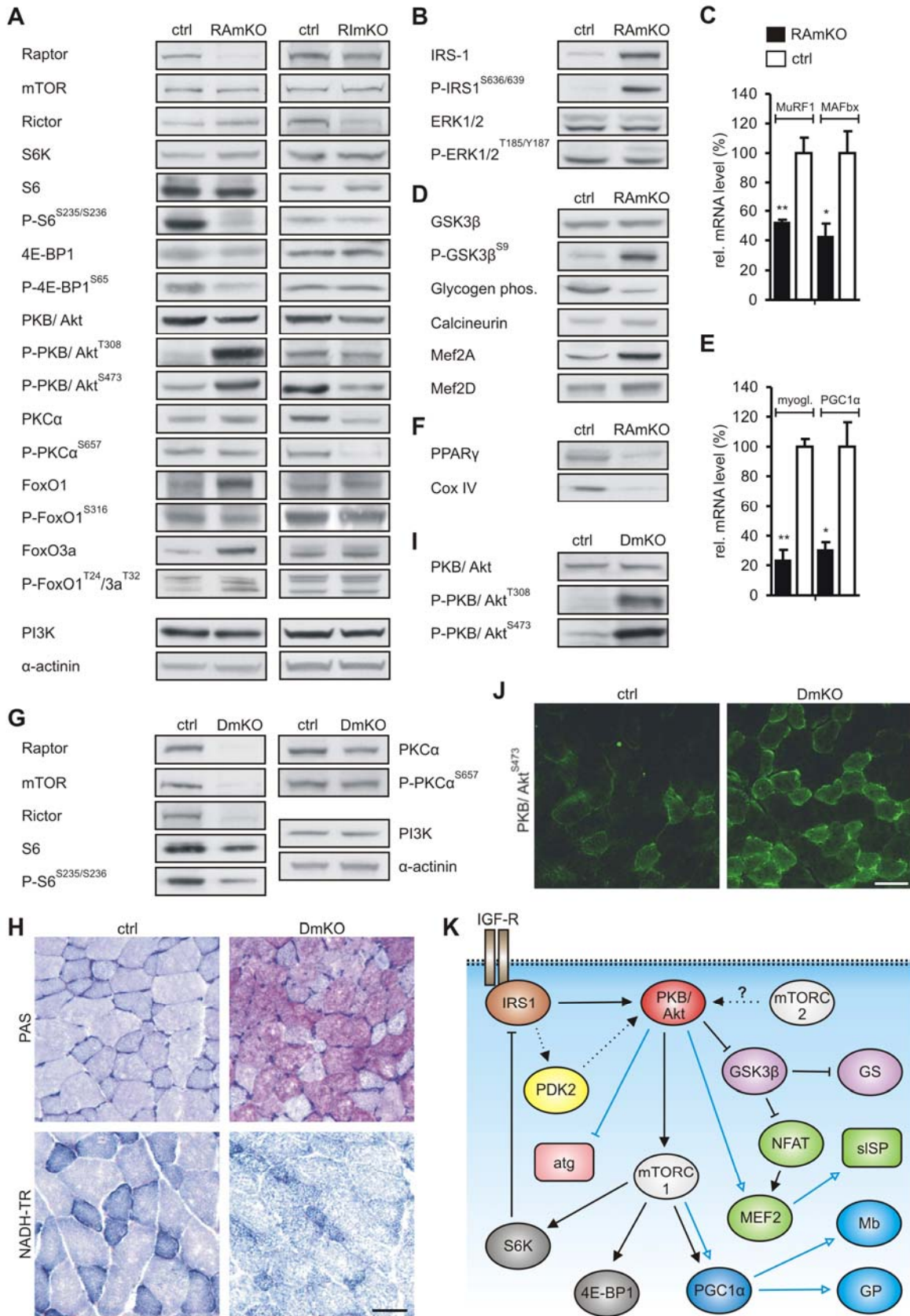


Figure 5. Biochemical characterization

(A,B,D,F) Western blot analysis of soleus muscle from 90 day-old RAmKO, RImKO and control mice using antibodies directed against the proteins indicated for details see Experimental Procedures. Equal amount of protein was loaded in each lane. Antibodies to α -actinin and PI3K were in addition used as loading controls.

(C & E) Relative mRNA levels of MuRF1, MAFbx, myoglobin myogl. and PGC1 α in soleus muscle of 90 day-old RAmKO or control mice. Values obtained in controls were set to 100% N = 3.

(G & I) Western blot analysis of soleus muscle from 60 day-old DmKO and control mice.

H PAS and NADH-TR staining on cross-sections of triceps muscles from 50 day-old DmKO and control mice.

(J) Immunostaining with antibodies specific for P-PKB/AKTS473 using cross-sections of 60 day-old DmKO and control mice.

(K) Schematic of the interactions contributing to the phenotype of RAmKO mice. Signaling pathway downstream of the insulin/IGF receptor is shown. Blue arrows with open arrowheads represent interactions that affect gene transcription; black symbols represent regulation on the protein level that activate or inhibit the targets. Abbreviations are: atg: atrogenes MuRF1 and MAFbx, GP: glycogen phosphorylase; GS: glycogen synthase; IGF-R: IGF receptor; Mb: myoglobin; sISP: slow structural proteins. Data C, E represent mean \pm SEM. Scale bars H, J: 50 μ m. P-values are: ** $p < 0.01$; * $p < 0.05$.

8. SUPPLEMENTAL FIGURES

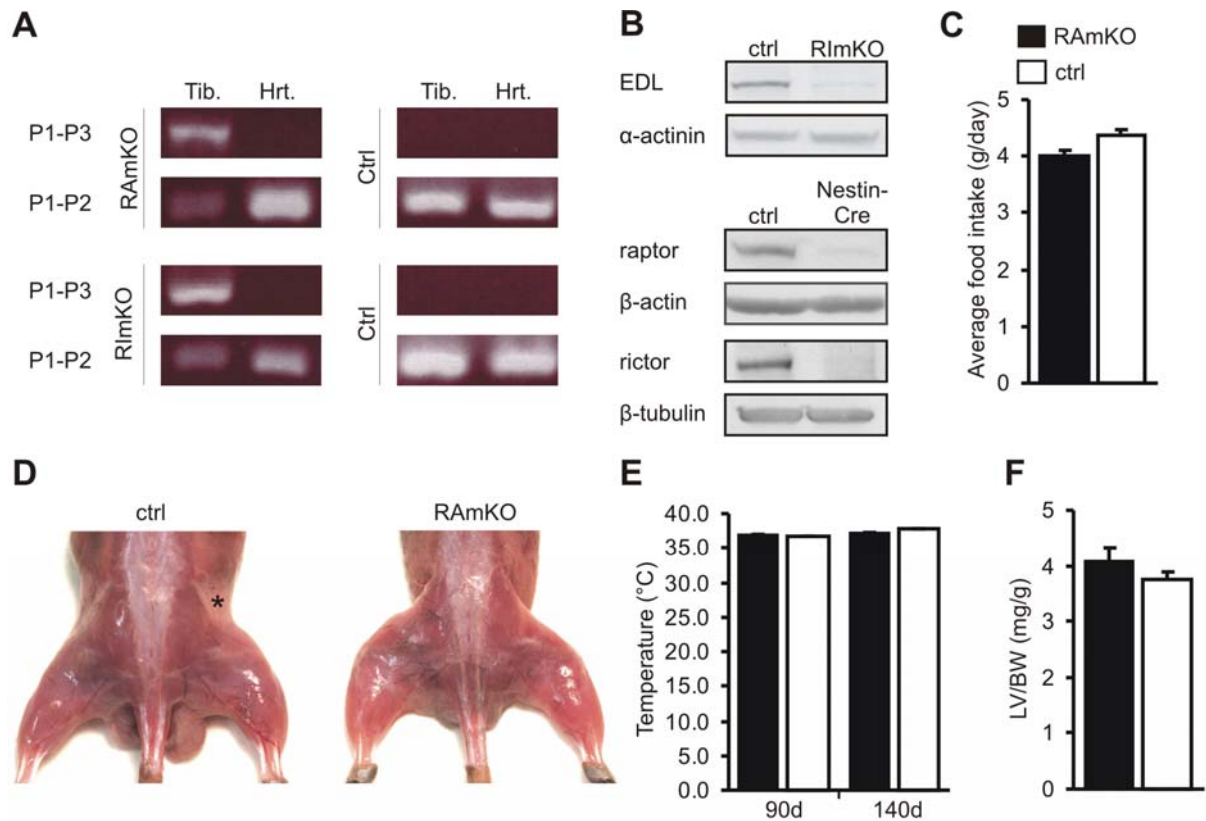


Figure S1. Specificity of recombination and characterization of RAmKO mice.

(A) PCR on 40 ng of genomic DNA extracted from *tibialis* muscle Tib. or the heart Hrt. of 60 day-old RAMKO, RImKO or control ctrl littermates. The PCR product indicating successful recombination by Cre recombinase primers P1 and P3, see Fig. 1A for details is only observed in *tibialis* muscle and not in the heart of RAMKO or RImKO mice. Note that as a result of recombination, less PCR product than in control mice was detected of the non-recombined locus P1-P2 primers.

(B) Western blot analysis of EDL muscle from 90 day-old RImKO and control mice and with brain lysates isolated from mice homozygously carrying either the floxed *rictor* or *raptor* alleles and expressing the Cre recombinase under control of the nestin promoter *Nestin-Cre*. α-actinin, β-actin and β-tubulin were used as loading controls.

(C) Average daily food intake of RAMKO and control ctrl mice between the age of 42 to 140 days N = 5 for RAMKO; N = 8 for controls.

(D) Dorsal view on a 140 day-old skinned, male RAMKO or control mouse. Hindleg muscles of the RAMKO mouse appear thinner and no fat pads asterisk in ctrl mouse can be detected.

(E) Basal body temperature measured at the age of 90 and 140 days does not differ between RAmKO and control mice N=4.

(F) Left ventricular mass divided by the total body weight LV/BW does not change between 140 day-old control and RAmKO mice N = 3 mice. Bars represent mean \pm SEM.

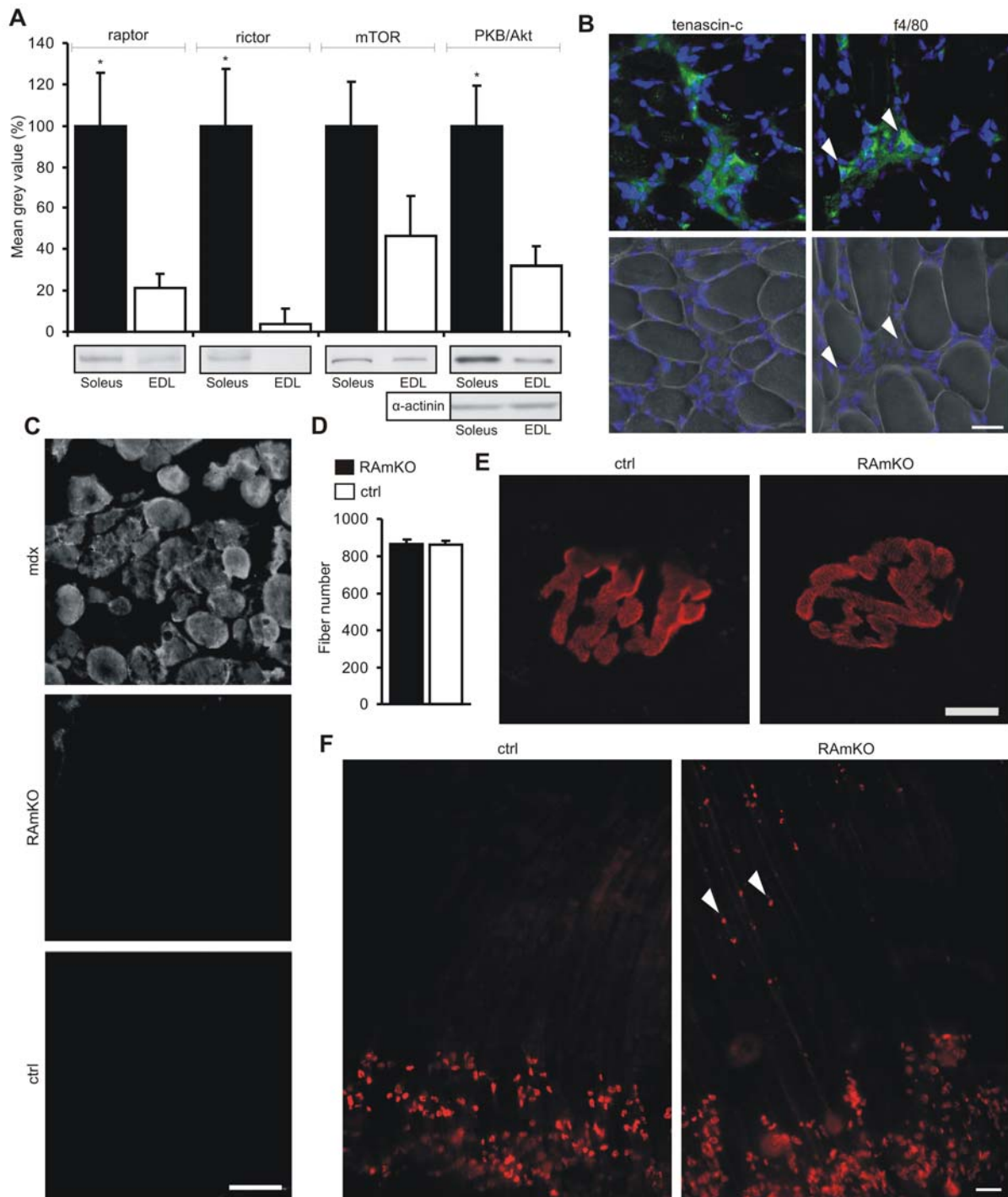


Figure S2. Expression pattern and assessment of muscular dystrophy parameters in RAmKO mice.

(A) Expression of selected proteins of the PKB/AKT and mTOR pathway in *soleus* and EDL muscle of wild-type C57/BL6 mice. Amount of total protein loaded was adjusted and additionally normalized to the levels of α -actinin. For quantification, grey values relative to α -actinin were measured for each protein and set to 100% for *soleus* N = 3 mice.

(B) Immunohistochemistry for tenascin-c and f4/80 green and DAPI staining blue reveals increased formation of fibrotic tissue and the presence of inflammatory monocytes white arrowheads in the *soleus* muscle of 140 day-old RAmKO mice.

(C) Evans blue dye EBD incorporation in the lower hindleg of 90 day-old RAmKO and control ctrl mice after 3 days of forced treadmill running. No EBD positive fibers could be found in control or RAmKO muscles. In mdx mice, which served as an experimental control, massive incorporation of EBD was observed.

(D) The number of fibers in the *soleus* of 180 day-old RAmKO mice is the same as in control littermates N=4.

(E) Maximal intensity projection using confocal microscopy of a whole mount preparation of neuromuscular junctions of the diaphragm of a 90 day-old control ctrl or RAmKO mouse. Acetylcholine receptors AChRs were visualized by TRITC-conjugated α -bungarotoxin. There is no difference between the two genotypes.

(F) Low magnification pictures of diaphragms of 90 day-old mice stained with TRITC- α -bungarotoxin. The innervation band can be discerned at the bottom of each picture. Extrasynaptic AChR clusters white arrowheads are found in the diaphragm of RAmKO mice. Bars represent mean \pm SEM. Scale bars = 50 μ m B & C, 10 μ m D, 100 μ m E. P-value: * $p < 0.05$.

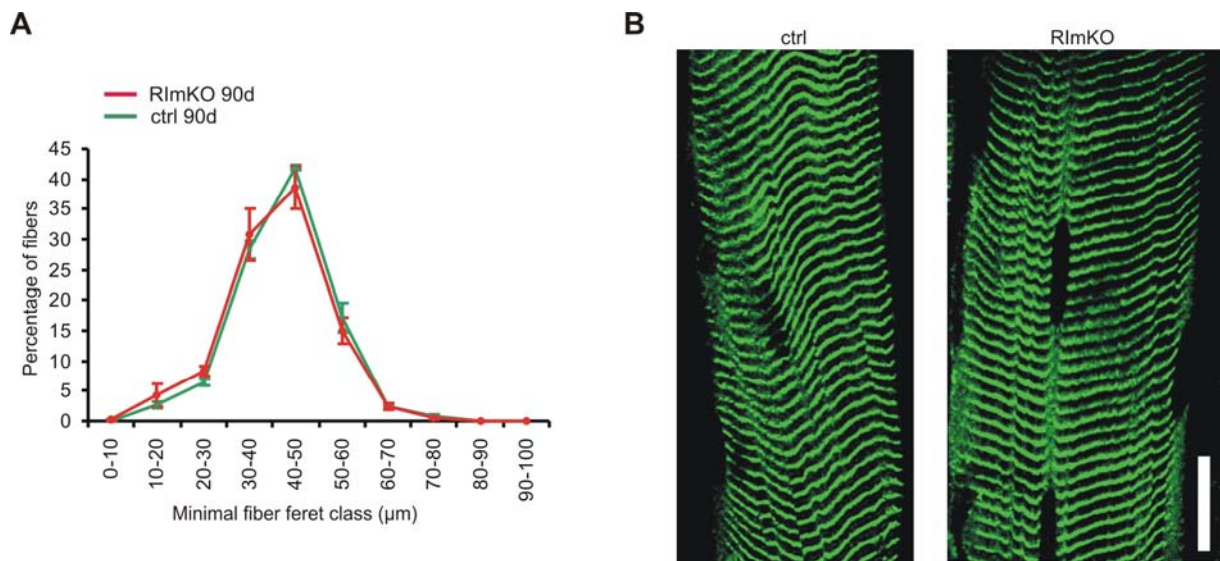


Figure S3. Fiber size distribution and cytoskeletal architecture in RImKO mice.

(A) Fiber size distribution in *soleus* muscle of 90 day-old RImKO and control mice. There is no difference between the two genotypes. Data points represent mean \pm SEM N = 3 mice.

(B) Maximal intensity projection using confocal microscopy of muscle fibers from 90 day-old mice stained with antibodies to α -actinin. No difference in the sarcomeric organization was observed. Scale bar = 20 μ m.

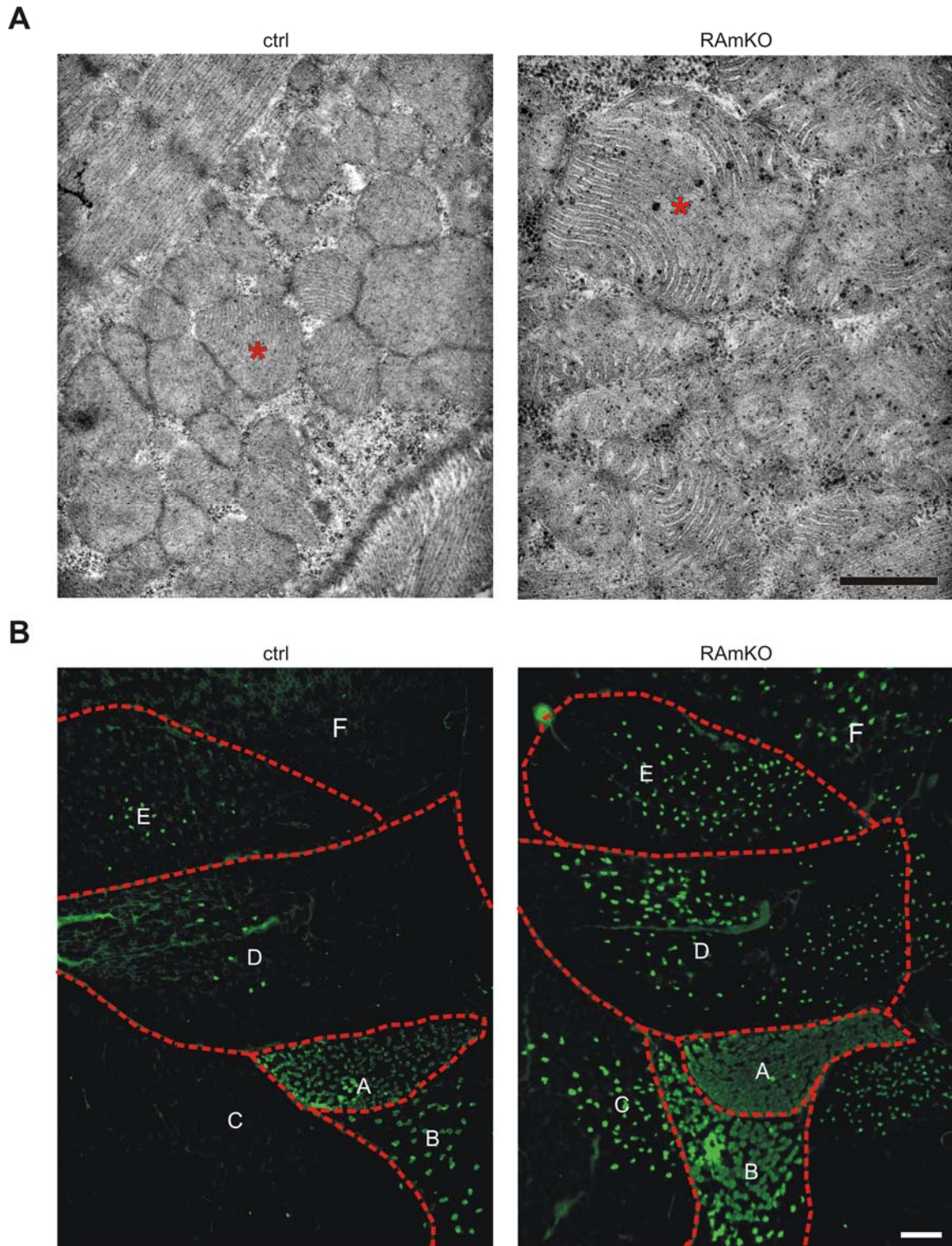


Figure S4. Subsarcolemmal accumulation of misshaped mitochondria and regionalized SIMHC expression in RAmKO mice.

(A) Representative high power electron micrographs of RAmKO and control ctrl *soleus* muscle. Subsarcolemmal mitochondria in RAmKO mice are morphologically abnormal asterisk marks a single mitochondrion and mitochondria are more densely packed than in control mice.

(B) Immunostaining for sIMHC green using cross-sections of the entire hindleg of RAmKO and control mice. Individual muscles are outlined by red, dotted lines. A: *soleus*; B: plantaris-adjacent *gastrocnemius*; C: *gastrocnemius*; D: *peroneus longus* and *peroneus brevis*; E: *extensor digitorum longus* EDL; F: *tibialis anterior*. Note that the expression of sIMHC in RAmKO mice is high in particular regions of muscles. Scale bars = 1 μ m A, 200 μ m B.

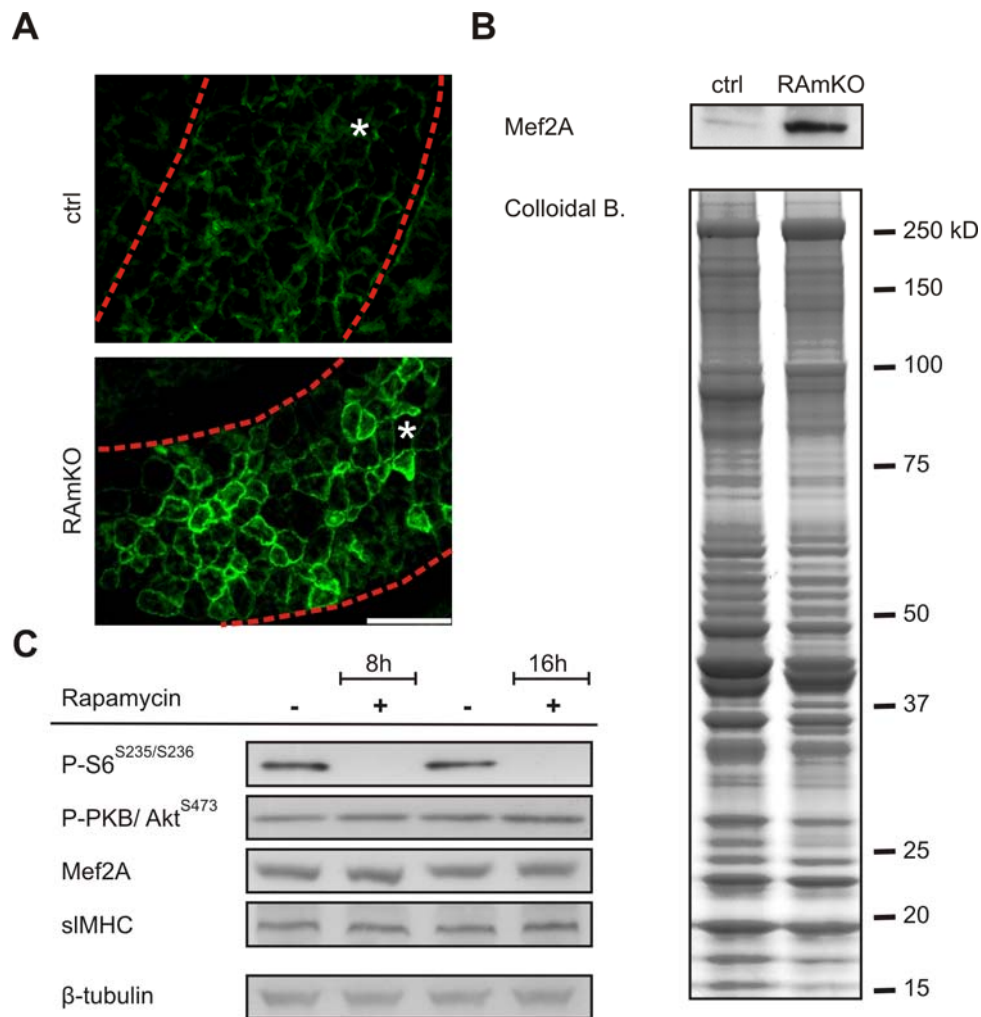


Figure S5. In-vivo and in-vitro alterations of Ser473-phosphorylated PKB/AKT, Mef2A and SIMHC.

(A) Cross-sections of the hindleg isolated from 90 day-old RAmKO or control ctrl mice were stained with antibodies directed against PKB/AKT phosphorylated on Ser473 P-PKB/AKT^{S473}. *Soleus* muscle asterisk shows particularly high levels of P-PKB/AKT^{S473} along the sarcolemmal membrane in RAmKO mice. Scale bar = 125 μ m.

(B) Western blot analysis of EDL muscle from 90 day-old RAmKO and control ctrl mice using antibodies to Mef2A. Amount of total protein loaded was adjusted and SDS gels were stained with colloidal blue bottom as a loading control. Levels of Mef2A are increased in RAmKO compared to control mice.

(C) Western blot analysis of C2C12 cells that were treated for either 8 or 16 hours with rapamycin. β -tubulin was used as a loading control. As determined by quantification of grey-values N=3, treatment of C2C12 cells with rapamycin for eight or sixteen hours caused a significant loss of S6 phosphorylation. A slight, non-significant increase in P-PKB/AKT^{S473} was observed after 16 hour treatment. None of the other proteins was changed.

9. SUPPLEMENTAL TABLE

	RAmKO	ctrl	ratio	number of replicates	RImKO	ctrl	ratio	number of replicates	DmKO	ctrl	ratio	number of replicates
Raptor	11 ±3*	61 ±11	0.2	3	42 ±1*	51 ±2	0.8	3	2 ±0.5*	35 ±11	0.06	3
mTOR	4 ±2	11 ±4	0.4	4	24 ±5	26 ±1	0.9	3	2 ±1*	17 ±5	0.1	3
Rictor	9 ±1	8 ±1	1.2	4	26 ±1*	59 ±7	0.4	3	17 ±4*	38 ±7	0.4	4
siMHC	42 ±0.5**	15 ±6	2.7	4								
siTnT	73 ±4***	36 ±2	2.0	4								
S6K	56 ±5**	27 ±3	2.1	3	24 ±4	90 ±1	0.3	3				
S6	82 ±35	114 ±12	0.7	3	35 ±5	29 ±6	1.2	3	7 ±3	14 ±6	0.5	3
P-S6 ^{S235/S236}	3 ±1*	21 ±5	0.1	6	19 ±8	57 ±24	0.3	4	21 ±8	44 ±16	0.5	3
4E-BP1	28 ±5	38 ±5	0.7	4	32 ±5	28 ±7	1.1	4				
P-4E-BP1 ^{S65}	4 ±2*	16 ±2	0.3	4	49 ±12	41 ±10	1.2	4				
PKB/ Akt	104 ±4	129 ±11	0.8	3	14 ±1	27 ±7	0.5	3	12 ±4	15 ±5	0.8	3
P-PKB/ Akt ^{T308}	9 ±3*	1 ±0.3	8	4	41 ±1*	55 ±3	0.7	3	24 ±6*	0.6 ±3	40	3
P-PKB/ Akt ^{S473}	9 ±1.5**	1 ±0.5	9.6	4	37 ±6**	98 ±11	0.4	3	22 ±5*	10 ±3	2.3	4
PKCα	31 ±5	25 ±3	1.2	5	11 ±3***	49 ±6	0.2	4	17 ±5	24 ±7	0.7	3
P-PKCα ^{S657}	26 ±9	40 ±7	0.6	6	6 ±1**	58 ±11	0.1	3	48 ±17	35 ±10	1.4	3
FOXO1	61 ±4***	20 ±3	3.1	3	27 ±3	17 ±8	1.6	3				
P-FOXO1 ^{S316}	29 ±10	37 ±7	0.8	5	62 ±5	62 ±11	1	3				
FOXO3	70 ±6***	22 ±3	3.3	4	38 ±6	34 ±3	0.9	4				
P-FOXO1/3 ^{T24/T23}	35 ±7* / 27 ±1	8 ±2 / 28 ±1	4.5 / 1	4	33 ±6 / 29 ±7	30 ±2 / 31 ±4	0.9 / 1.1	4				
IRS-1	74 ±6***	11 ±1	6.7	3								
P-IRS-1 ^{S636/639}	41 ±14**	3 ±1	13.7	4								
ERK1/2	104 ±10 / 59 ±13	86 ±3 / 29 ±4	1.2 / 2	3								
P-ERK1/2 ^{T185/Y187}	3 ±1.5 / 16 ±2	2 ±0.5 / 18 ±4	2 / 0.9	3								
GSK3β	80 ±4	69 ±4	1.2	3								
P-GSK3β ^{S9}	39 ±13*	8 ±1	4.9	3								
Glycogen phos.	15 ±7*	51 ±7	0.3	3								
Calcineurin	31 ±4	21 ±2	1.5	4								
Mef2A	126 ±12*	64 ±11	2	3								
Mef2D	36 ±3	30 ±5	1.2	4								
PPARγ	19 ±3**	41 ±3	0.5	3								
COX IV	10 ±2**	20 ±2	0.5	6								

* p<0.05, ** p<0.01, ***p<0.001

Supplementary Table S1. Quantification of Western blot analysis for the proteins indicated. Proteins analyzed were extracted from *soleus* muscle of 90 day-old RAmKO, RImKO or control ctrl littermates. For the analysis of the DmKO mice, 60 day-old mice were compared with control littermates. Amount of total protein loaded onto the SDS-PAGE was adjusted and Western blots were additionally normalized with antibodies to α -actinin. Numbers given represent average grey values \pm SEM after subtraction of the background. "Ratio" represents the average grey value obtained from a knockout animal divided by the grey values from the control littermates. "Number of replicates" represents the number of knockout animals analyzed. The number of control littermates was always the same or higher than the values given. P-values were determined by student's t-test.

10. REFERENCES

1. Warren, S., *The immediate cause of death in cancer*. Am. J. Med. Sci., 1932(184): p. 610–613.
2. Janssen, I., et al., *The healthcare costs of sarcopenia in the United States*. J Am Geriatr Soc, 2004. **52**(1): p. 80-5.
3. Hahn, V., et al., *Physical activity and the metabolic syndrome in elderly German men and women: Results from the population based KORA survey*. Diabetes Care, 2008.
4. Musaro, A., et al., *Localized Igf-1 transgene expression sustains hypertrophy and regeneration in senescent skeletal muscle*. Nat Genet, 2001. **27**(2): p. 195-200.
5. Chen, W.S., et al., *Growth retardation and increased apoptosis in mice with homozygous disruption of the Akt1 gene*. Genes Dev, 2001. **15**(17): p. 2203-8.
6. Izumiya, Y., et al., *Fast/Glycolytic muscle fiber growth reduces fat mass and improves metabolic parameters in obese mice*. Cell Metab, 2008. **7**(2): p. 159-72.
7. Pallafacchina, G., et al., *A protein kinase B-dependent and rapamycin-sensitive pathway controls skeletal muscle growth but not fiber type specification*. Proc Natl Acad Sci U S A, 2002. **99**(14): p. 9213-8.
8. Bodine, S.C., et al., *Akt/mTOR pathway is a crucial regulator of skeletal muscle hypertrophy and can prevent muscle atrophy in vivo*. Nat Cell Biol, 2001. **3**(11): p. 1014-9.
9. Ohanna, M., et al., *Atrophy of S6K1(-/-) skeletal muscle cells reveals distinct mTOR effectors for cell cycle and size control*. Nat Cell Biol, 2005. **7**(3): p. 286-94.
10. Wan, M., et al., *Muscle atrophy in transgenic mice expressing a human TSC1 transgene*. FEBS Lett, 2006. **580**(24): p. 5621-7.
11. Guertin, D.A., et al., *Ablation in mice of the mTORC components raptor, rictor, or mLST8 reveals that mTORC2 is required for signaling to Akt-FOXO and PKCalpha, but not S6K1*. Dev Cell, 2006. **11**(6): p. 859-71.
12. Shiota, C., et al., *Multiallelic disruption of the rictor gene in mice reveals that mTOR complex 2 is essential for fetal growth and viability*. Dev Cell, 2006. **11**(4): p. 583-9.
13. Gangloff, Y.G., et al., *Disruption of the mouse mTOR gene leads to early postimplantation lethality and prohibits embryonic stem cell development*. Mol Cell Biol, 2004. **24**(21): p. 9508-16.
14. Kaplan, S.A. and P. Cohen, *The somatomedin hypothesis 2007: 50 years later*. J Clin Endocrinol Metab, 2007. **92**(12): p. 4529-35.
15. Gelato, M., M. McNurlan, and E. Freedland, *Role of recombinant human growth hormone in HIV-associated wasting and cachexia: pathophysiology and rationale for treatment*. Clin Ther, 2007. **29**(11): p. 2269-88.
16. Ellis, K.J., et al., *Changes in body composition of human immunodeficiency virus-infected males receiving insulin-like growth factor I and growth hormone*. J Clin Endocrinol Metab, 1996. **81**(8): p. 3033-8.
17. Bessey, P.Q., et al., *Posttraumatic skeletal muscle proteolysis: the role of the hormonal environment*. World J Surg, 1989. **13**(4): p. 465-70; discussion 471.
18. Monk, D.N., et al., *Sequential changes in the metabolic response in critically injured patients during the first 25 days after blunt trauma*. Ann Surg, 1996. **223**(4): p. 395-405.
19. Byrne, T.A., et al., *Anabolic therapy with growth hormone accelerates protein gain in surgical patients requiring nutritional rehabilitation*. Ann Surg, 1993. **218**(4): p. 400-16; discussion 416-8.
20. Gore, D.C., et al., *Effect of exogenous growth hormone on whole-body and isolated-limb protein kinetics in burned patients*. Arch Surg, 1991. **126**(1): p. 38-43.
21. Hart, D.W., et al., *Attenuation of posttraumatic muscle catabolism and osteopenia by long-term growth hormone therapy*. Ann Surg, 2001. **233**(6): p. 827-34.
22. Wolfson, L., et al., *Strength is a major factor in balance, gait, and the occurrence of falls*. J Gerontol A Biol Sci Med Sci, 1995. **50 Spec No**: p. 64-7.
23. Corpas, E., S.M. Harman, and M.R. Blackman, *Human growth hormone and human aging*. Endocr Rev, 1993. **14**(1): p. 20-39.
24. Iranmanesh, A., G. Lizarralde, and J.D. Veldhuis, *Age and relative adiposity are specific negative determinants of the frequency and amplitude of growth hormone (GH) secretory bursts and the half-life of endogenous GH in healthy men*. J Clin Endocrinol Metab, 1991. **73**(5): p. 1081-8.
25. Borst, S.E., *Interventions for sarcopenia and muscle weakness in older people*. Age Ageing, 2004. **33**(6): p. 548-55.

26. Renehan, A.G. and B.M. Brennan, *Acromegaly, growth hormone and cancer risk*. Best Pract Res Clin Endocrinol Metab, 2008. **22**(4): p. 639-57.
27. Wu, Y., et al., *Circulating insulin-like growth factor-I levels regulate colon cancer growth and metastasis*. Cancer Res, 2002. **62**(4): p. 1030-5.
28. Hedekov, C.J., *Mechanism of glucose-induced insulin secretion*. Physiol Rev, 1980. **60**(2): p. 442-509.
29. Flati, V., et al., *Intracellular mechanisms of metabolism regulation: the role of signaling via the mammalian target of rapamycin pathway and other routes*. Am J Cardiol, 2008. **101**(11A): p. 16E-21E.
30. Sancak, Y., et al., *The Rag GTPases bind raptor and mediate amino acid signaling to mTORC1*. Science, 2008. **320**(5882): p. 1496-501.
31. Hara, K., et al., *Amino acid sufficiency and mTOR regulate p70 S6 kinase and eIF-4E BP1 through a common effector mechanism*. J Biol Chem, 1998. **273**(23): p. 14484-94.
32. Pansarasa, O., et al., *Oral amino acid supplementation counteracts age-induced sarcopenia in elderly rats*. Am J Cardiol, 2008. **101**(11A): p. 35E-41E.
33. Negro, M., et al., *Branched-chain amino acid supplementation does not enhance athletic performance but affects muscle recovery and the immune system*. J Sports Med Phys Fitness, 2008. **48**(3): p. 347-51.
34. Rennie, M.J., et al., *Branched-chain amino acids as fuels and anabolic signals in human muscle*. J Nutr, 2006. **136**(1 Suppl): p. 264S-8S.
35. Gleason, C.E., et al., *The role of AMPK and mTOR in nutrient sensing in pancreatic beta-cells*. J Biol Chem, 2007. **282**(14): p. 10341-51.
36. Hardwick, J.S., et al., *Rapamycin-modulated transcription defines the subset of nutrient-sensitive signaling pathways directly controlled by the Tor proteins*. Proc Natl Acad Sci U S A, 1999. **96**(26): p. 14866-70.
37. Peng, T., T.R. Golub, and D.M. Sabatini, *The immunosuppressant rapamycin mimics a starvation-like signal distinct from amino acid and glucose deprivation*. Mol Cell Biol, 2002. **22**(15): p. 5575-84.
38. Edinger, A.L., et al., *Differential effects of rapamycin on mammalian target of rapamycin signaling functions in mammalian cells*. Cancer Res, 2003. **63**(23): p. 8451-60.
39. Schieke, S.M., et al., *The mammalian target of rapamycin (mTOR) pathway regulates mitochondrial oxygen consumption and oxidative capacity*. J Biol Chem, 2006. **281**(37): p. 27643-52.
40. Cunningham, J.T., et al., *mTOR controls mitochondrial oxidative function through a YY1-PGC-1alpha transcriptional complex*. Nature, 2007. **450**(7170): p. 736-40.
41. Sandri, M., et al., *PGC-1alpha protects skeletal muscle from atrophy by suppressing FoxO3 action and atrophy-specific gene transcription*. Proc Natl Acad Sci U S A, 2006. **103**(44): p. 16260-5.
42. Akimoto, T., et al., *Exercise stimulates Pgc-1alpha transcription in skeletal muscle through activation of the p38 MAPK pathway*. J Biol Chem, 2005. **280**(20): p. 19587-93.
43. Owen, N., A. Bauman, and W. Brown, *Too Much Sitting: A Novel and Important Predictor of Chronic Disease Risk?* Br J Sports Med, 2008.
44. Achten, J. and A.E. Jeukendrup, *Optimizing fat oxidation through exercise and diet*. Nutrition, 2004. **20**(7-8): p. 716-27.
45. Benziane, B., et al., *Divergent cell signaling after short-term intensified endurance training in human skeletal muscle*. Am J Physiol Endocrinol Metab, 2008. **295**(6): p. E1427-38.
46. Zhao, J., et al., *FoxO3 coordinately activates protein degradation by the autophagic/lysosomal and proteasomal pathways in atrophying muscle cells*. Cell Metab, 2007. **6**(6): p. 472-83.
47. Klionsky, D.J., *Autophagy: from phenomenology to molecular understanding in less than a decade*. Nat Rev Mol Cell Biol, 2007. **8**(11): p. 931-7.
48. DeVol, D.L., et al., *Activation of insulin-like growth factor gene expression during work-induced skeletal muscle growth*. Am J Physiol, 1990. **259**(1 Pt 1): p. E89-95.
49. Goldspink, G., *Mechanical signals, IGF-I gene splicing, and muscle adaptation*. Physiology (Bethesda), 2005. **20**: p. 232-8.
50. Rommel, C., et al., *Mediation of IGF-1-induced skeletal myotube hypertrophy by PI(3)K/Akt/mTOR and PI(3)K/Akt/GSK3 pathways*. Nat Cell Biol, 2001. **3**(11): p. 1009-13.
51. Sano, H., et al., *Insulin-stimulated phosphorylation of a Rab GTPase-activating protein regulates GLUT4 translocation*. J Biol Chem, 2003. **278**(17): p. 14599-602.
52. Eguez, L., et al., *Full intracellular retention of GLUT4 requires AS160 Rab GTPase activating protein*. Cell Metab, 2005. **2**(4): p. 263-72.

53. Kohn, A.D., et al., *Expression of a constitutively active Akt Ser/Thr kinase in 3T3-L1 adipocytes stimulates glucose uptake and glucose transporter 4 translocation*. J Biol Chem, 1996. **271**(49): p. 31372-8.
54. Martin, D.E. and M.N. Hall, *The expanding TOR signaling network*. Curr Opin Cell Biol, 2005. **17**(2): p. 158-66.
55. Takei, N., et al., *Brain-derived neurotrophic factor induces mammalian target of rapamycin-dependent local activation of translation machinery and protein synthesis in neuronal dendrites*. J Neurosci, 2004. **24**(44): p. 9760-9.
56. Inoki, K., T. Zhu, and K.L. Guan, *TSC2 mediates cellular energy response to control cell growth and survival*. Cell, 2003. **115**(5): p. 577-90.
57. Jacinto, E. and M.N. Hall, *Tor signalling in bugs, brain and brawn*. Nat Rev Mol Cell Biol, 2003. **4**(2): p. 117-26.
58. Lin, J., et al., *Transcriptional co-activator PGC-1 alpha drives the formation of slow-twitch muscle fibres*. Nature, 2002. **418**(6899): p. 797-801.
59. Jacinto, E., et al., *Mammalian TOR complex 2 controls the actin cytoskeleton and is rapamycin insensitive*. Nat Cell Biol, 2004. **6**(11): p. 1122-8.
60. Sarbassov, D.D., et al., *Rictor, a novel binding partner of mTOR, defines a rapamycin-insensitive and raptor-independent pathway that regulates the cytoskeleton*. Curr Biol, 2004. **14**(14): p. 1296-302.
61. Loewith, R., et al., *Two TOR complexes, only one of which is rapamycin sensitive, have distinct roles in cell growth control*. Mol Cell, 2002. **10**(3): p. 457-68.
62. Kim, D.H., et al., *mTOR interacts with raptor to form a nutrient-sensitive complex that signals to the cell growth machinery*. Cell, 2002. **110**(2): p. 163-75.
63. Hara, K., et al., *Raptor, a binding partner of target of rapamycin (TOR), mediates TOR action*. Cell, 2002. **110**(2): p. 177-89.
64. Choi, K.M., L.P. McMahon, and J.C. Lawrence, Jr., *Two motifs in the translational repressor PHAS-I required for efficient phosphorylation by mammalian target of rapamycin and for recognition by raptor*. J Biol Chem, 2003. **278**(22): p. 19667-73.
65. Nojima, H., et al., *The mammalian target of rapamycin (mTOR) partner, raptor, binds the mTOR substrates p70 S6 kinase and 4E-BP1 through their TOR signaling (TOS) motif*. J Biol Chem, 2003. **278**(18): p. 15461-4.
66. Schalm, S.S., et al., *TOS motif-mediated raptor binding regulates 4E-BP1 multisite phosphorylation and function*. Curr Biol, 2003. **13**(10): p. 797-806.
67. Oshiro, N., et al., *Dissociation of raptor from mTOR is a mechanism of rapamycin-induced inhibition of mTOR function*. Genes Cells, 2004. **9**(4): p. 359-66.
68. Kim, D.H., et al., *GbetaL, a positive regulator of the rapamycin-sensitive pathway required for the nutrient-sensitive interaction between raptor and mTOR*. Mol Cell, 2003. **11**(4): p. 895-904.
69. Thedieck, K., et al., *PRAS40 and PRR5-like protein are new mTOR interactors that regulate apoptosis*. PLoS ONE, 2007. **2**(11): p. e1217.
70. Sancak, Y., et al., *PRAS40 is an insulin-regulated inhibitor of the mTORC1 protein kinase*. Mol Cell, 2007. **25**(6): p. 903-15.
71. Sarbassov, D.D., et al., *Phosphorylation and regulation of Akt/PKB by the rictor-mTOR complex*. Science, 2005. **307**(5712): p. 1098-101.
72. Frias, M.A., et al., *mSin1 is necessary for Akt/PKB phosphorylation, and its isoforms define three distinct mTORC2s*. Curr Biol, 2006. **16**(18): p. 1865-70.
73. Woo, S.Y., et al., *PRR5, a novel component of mTOR complex 2, regulates platelet-derived growth factor receptor beta expression and signaling*. J Biol Chem, 2007. **282**(35): p. 25604-12.
74. Pearce, L.R., et al., *Identification of Protor as a novel Rictor-binding component of mTOR complex-2*. Biochem J, 2007. **405**(3): p. 513-22.
75. Huang, J., et al., *The TSC1-TSC2 complex is required for proper activation of mTOR complex 2*. Mol Cell Biol, 2008. **28**(12): p. 4104-15.
76. Murakami, M., et al., *mTOR is essential for growth and proliferation in early mouse embryos and embryonic stem cells*. Mol Cell Biol, 2004. **24**(15): p. 6710-8.
77. Franke, T.F., *PI3K/Akt: getting it right matters*. Oncogene, 2008. **27**(50): p. 6473-88.
78. Dong, L.Q. and F. Liu, *PDK2: the missing piece in the receptor tyrosine kinase signaling pathway puzzle*. Am J Physiol Endocrinol Metab, 2005. **289**(2): p. E187-96.
79. Bozulic, L., et al., *PKBalpha/Akt1 Acts Downstream of DNA-PK in the DNA Double-Strand Break Response and Promotes Survival*. Mol Cell, 2008. **30**(2): p. 203-13.
80. Manning, B.D. and L.C. Cantley, *AKT/PKB signaling: navigating downstream*. Cell, 2007. **129**(7): p. 1261-74.

81. Gao, X. and D. Pan, *TSC1 and TSC2 tumor suppressors antagonize insulin signaling in cell growth*. Genes Dev, 2001. **15**(11): p. 1383-92.
82. Goncharova, E., et al., *TSC2 modulates actin cytoskeleton and focal adhesion through TSC1-binding domain and the Rac1 GTPase*. J Cell Biol, 2004. **167**(6): p. 1171-82.
83. Tapon, N., et al., *The Drosophila tuberous sclerosis complex gene homologs restrict cell growth and cell proliferation*. Cell, 2001. **105**(3): p. 345-55.
84. Inoki, K., et al., *TSC2 is phosphorylated and inhibited by Akt and suppresses mTOR signalling*. Nat Cell Biol, 2002. **4**(9): p. 648-57.
85. Manning, B.D., et al., *Identification of the tuberous sclerosis complex-2 tumor suppressor gene product tuberin as a target of the phosphoinositide 3-kinase/akt pathway*. Mol Cell, 2002. **10**(1): p. 151-62.
86. Potter, C.J., L.G. Pedraza, and T. Xu, *Akt regulates growth by directly phosphorylating Tsc2*. Nat Cell Biol, 2002. **4**(9): p. 658-65.
87. Kovacina, K.S., et al., *Identification of a proline-rich Akt substrate as a 14-3-3 binding partner*. J Biol Chem, 2003. **278**(12): p. 10189-94.
88. Cross, D.A., et al., *Inhibition of glycogen synthase kinase-3 by insulin mediated by protein kinase B*. Nature, 1995. **378**(6559): p. 785-9.
89. Datta, S.R., et al., *Akt phosphorylation of BAD couples survival signals to the cell-intrinsic death machinery*. Cell, 1997. **91**(2): p. 231-41.
90. del Peso, L., et al., *Interleukin-3-induced phosphorylation of BAD through the protein kinase Akt*. Science, 1997. **278**(5338): p. 687-9.
91. Mayo, L.D. and D.B. Donner, *A phosphatidylinositol 3-kinase/Akt pathway promotes translocation of Mdm2 from the cytoplasm to the nucleus*. Proc Natl Acad Sci U S A, 2001. **98**(20): p. 11598-603.
92. Zhou, B.P., et al., *HER-2/neu induces p53 ubiquitination via Akt-mediated MDM2 phosphorylation*. Nat Cell Biol, 2001. **3**(11): p. 973-82.
93. Cardone, M.H., et al., *Regulation of cell death protease caspase-9 by phosphorylation*. Science, 1998. **282**(5392): p. 1318-21.
94. Olsson, A.K., et al., *VEGF receptor signalling - in control of vascular function*. Nat Rev Mol Cell Biol, 2006. **7**(5): p. 359-71.
95. Tran, H., et al., *The many forks in FOXO's road*. Sci STKE, 2003. **2003**(172): p. RE5.
96. Dimmeler, S., et al., *Activation of nitric oxide synthase in endothelial cells by Akt-dependent phosphorylation*. Nature, 1999. **399**(6736): p. 601-5.
97. Fulton, D., et al., *Regulation of endothelium-derived nitric oxide production by the protein kinase Akt*. Nature, 1999. **399**(6736): p. 597-601.
98. Lai, K.M., et al., *Conditional activation of akt in adult skeletal muscle induces rapid hypertrophy*. Mol Cell Biol, 2004. **24**(21): p. 9295-304.
99. Gao, X., et al., *Tsc tumour suppressor proteins antagonize amino-acid-TOR signalling*. Nat Cell Biol, 2002. **4**(9): p. 699-704.
100. Goncharova, E.A., et al., *Tuberin regulates p70 S6 kinase activation and ribosomal protein S6 phosphorylation. A role for the TSC2 tumor suppressor gene in pulmonary lymphangiomyomatosis (LAM)*. J Biol Chem, 2002. **277**(34): p. 30958-67.
101. Jaeschke, A., et al., *Tuberous sclerosis complex tumor suppressor-mediated S6 kinase inhibition by phosphatidylinositide-3-OH kinase is mTOR independent*. J Cell Biol, 2002. **159**(2): p. 217-24.
102. Tee, A.R., et al., *Tuberous sclerosis complex-1 and -2 gene products function together to inhibit mammalian target of rapamycin (mTOR)-mediated downstream signaling*. Proc Natl Acad Sci U S A, 2002. **99**(21): p. 13571-6.
103. Kwiatkowski, D.J., et al., *A mouse model of TSC1 reveals sex-dependent lethality from liver hemangiomas, and up-regulation of p70S6 kinase activity in Tsc1 null cells*. Hum Mol Genet, 2002. **11**(5): p. 525-34.
104. Zhang, Y., et al., *Rheb is a direct target of the tuberous sclerosis tumour suppressor proteins*. Nat Cell Biol, 2003. **5**(6): p. 578-81.
105. Inoki, K., et al., *Rheb GTPase is a direct target of TSC2 GAP activity and regulates mTOR signaling*. Genes Dev, 2003. **17**(15): p. 1829-34.
106. Tee, A.R., et al., *Tuberous sclerosis complex gene products, Tuberin and Hamartin, control mTOR signaling by acting as a GTPase-activating protein complex toward Rheb*. Curr Biol, 2003. **13**(15): p. 1259-68.
107. Castro, A.F., et al., *Rheb binds tuberous sclerosis complex 2 (TSC2) and promotes S6 kinase activation in a rapamycin- and farnesylation-dependent manner*. J Biol Chem, 2003. **278**(35): p. 32493-6.

108. Tee, A.R., R. Anjum, and J. Blenis, *Inactivation of the tuberous sclerosis complex-1 and -2 gene products occurs by phosphoinositide 3-kinase/Akt-dependent and -independent phosphorylation of tuberin*. J Biol Chem, 2003. **278**(39): p. 37288-96.
109. Roux, P.P., et al., *Tumor-promoting phorbol esters and activated Ras inactivate the tuberous sclerosis tumor suppressor complex via p90 ribosomal S6 kinase*. Proc Natl Acad Sci U S A, 2004. **101**(37): p. 13489-94.
110. Lee, D.F., et al., *IKK beta suppression of TSC1 links inflammation and tumor angiogenesis via the mTOR pathway*. Cell, 2007. **130**(3): p. 440-55.
111. Shaw, R.J., et al., *The LKB1 tumor suppressor negatively regulates mTOR signaling*. Cancer Cell, 2004. **6**(1): p. 91-9.
112. Inoki, K., et al., *TSC2 integrates Wnt and energy signals via a coordinated phosphorylation by AMPK and GSK3 to regulate cell growth*. Cell, 2006. **126**(5): p. 955-68.
113. Polakis, P., *The many ways of Wnt in cancer*. Curr Opin Genet Dev, 2007. **17**(1): p. 45-51.
114. Arsham, A.M., J.J. Howell, and M.C. Simon, *A novel hypoxia-inducible factor-independent hypoxic response regulating mammalian target of rapamycin and its targets*. J Biol Chem, 2003. **278**(32): p. 29655-60.
115. Brugarolas, J., et al., *Regulation of mTOR function in response to hypoxia by REDD1 and the TSC1/TSC2 tumor suppressor complex*. Genes Dev, 2004. **18**(23): p. 2893-904.
116. Hay, N. and N. Sonenberg, *Upstream and downstream of mTOR*. Genes Dev, 2004. **18**(16): p. 1926-45.
117. Tee, A.R. and J. Blenis, *mTOR, translational control and human disease*. Semin Cell Dev Biol, 2005. **16**(1): p. 29-37.
118. Mieulet, V., et al., *S6 kinase inactivation impairs growth and translational target phosphorylation in muscle cells maintaining proper regulation of protein turnover*. Am J Physiol Cell Physiol, 2007. **293**(2): p. C712-22.
119. Um, S.H., et al., *Absence of S6K1 protects against age- and diet-induced obesity while enhancing insulin sensitivity*. Nature, 2004. **431**(7005): p. 200-5.
120. Teleanu, A.A., Y.W. Chen, and S.M. Cohen, *4E-BP functions as a metabolic brake used under stress conditions but not during normal growth*. Genes Dev, 2005. **19**(16): p. 1844-8.
121. Tsukiyama-Kohara, K., et al., *Adipose tissue reduction in mice lacking the translational inhibitor 4E-BP1*. Nat Med, 2001. **7**(10): p. 1128-32.
122. Cardenas, M.E., et al., *The TOR signaling cascade regulates gene expression in response to nutrients*. Genes Dev, 1999. **13**(24): p. 3271-9.
123. Shamji, A.F., F.G. Kuruvilla, and S.L. Schreiber, *Partitioning the transcriptional program induced by rapamycin among the effectors of the Tor proteins*. Curr Biol, 2000. **10**(24): p. 1574-81.
124. Nakashima, S., *Protein kinase C alpha (PKC alpha): regulation and biological function*. J Biochem, 2002. **132**(5): p. 669-75.
125. Jacinto, E., et al., *SIN1/MIP1 maintains rictor-mTOR complex integrity and regulates Akt phosphorylation and substrate specificity*. Cell, 2006. **127**(1): p. 125-37.
126. Polak, P. and M.N. Hall, *mTORC2 Caught in a SINful Akt*. Dev Cell, 2006. **11**(4): p. 433-4.
127. Haruta, T., et al., *A rapamycin-sensitive pathway down-regulates insulin signaling via phosphorylation and proteasomal degradation of insulin receptor substrate-1*. Mol Endocrinol, 2000. **14**(6): p. 783-94.
128. Tremblay, F. and A. Marette, *Amino acid and insulin signaling via the mTOR/p70 S6 kinase pathway. A negative feedback mechanism leading to insulin resistance in skeletal muscle cells*. J Biol Chem, 2001. **276**(41): p. 38052-60.
129. Berg, C.E., B.E. Lavan, and C.M. Rondinone, *Rapamycin partially prevents insulin resistance induced by chronic insulin treatment*. Biochem Biophys Res Commun, 2002. **293**(3): p. 1021-7.
130. Hartley, D. and G.M. Cooper, *Role of mTOR in the degradation of IRS-1: regulation of PP2A activity*. J Cell Biochem, 2002. **85**(2): p. 304-14.
131. Zhande, R., et al., *Molecular mechanism of insulin-induced degradation of insulin receptor substrate 1*. Mol Cell Biol, 2002. **22**(4): p. 1016-26.
132. Greene, M.W., et al., *Modulation of insulin-stimulated degradation of human insulin receptor substrate-1 by Serine 312 phosphorylation*. J Biol Chem, 2003. **278**(10): p. 8199-211.
133. Pirola, L., et al., *Phosphoinositide 3-kinase-mediated reduction of insulin receptor substrate-1/2 protein expression via different mechanisms contributes to the insulin-induced desensitization of its signaling pathways in L6 muscle cells*. J Biol Chem, 2003. **278**(18): p. 15641-51.
134. Harrington, L.S., et al., *The TSC1-2 tumor suppressor controls insulin-PI3K signaling via regulation of IRS proteins*. J Cell Biol, 2004. **166**(2): p. 213-23.

135. Shah, O.J. and T. Hunter, *Critical role of T-loop and H-motif phosphorylation in the regulation of S6 kinase 1 by the tuberous sclerosis complex*. J Biol Chem, 2004. **279**(20): p. 20816-23.
136. Tremblay, F., et al., *Identification of IRS-1 Ser-1101 as a target of S6K1 in nutrient- and obesity-induced insulin resistance*. Proc Natl Acad Sci U S A, 2007. **104**(35): p. 14056-61.
137. Ozes, O.N., et al., *A phosphatidylinositol 3-kinase/Akt/mTOR pathway mediates and PTEN antagonizes tumor necrosis factor inhibition of insulin signaling through insulin receptor substrate-1*. Proc Natl Acad Sci U S A, 2001. **98**(8): p. 4640-5.
138. Tzatsos, A. and P.N. Tsiachlis, *Energy depletion inhibits phosphatidylinositol 3-kinase/Akt signaling and induces apoptosis via AMP-activated protein kinase-dependent phosphorylation of IRS-1 at Ser-794*. J Biol Chem, 2007. **282**(25): p. 18069-82.
139. O'Reilly, K.E., et al., *mTOR inhibition induces upstream receptor tyrosine kinase signaling and activates Akt*. Cancer Res, 2006. **66**(3): p. 1500-8.
140. Baselga, J., *Novel agents in the era of targeted therapy: what have we learned and how has our practice changed?* Ann Oncol, 2008. **19 Suppl 7**: p. vii281-8.
141. Cloughesy, T.F., et al., *Antitumor activity of rapamycin in a Phase I trial for patients with recurrent PTEN-deficient glioblastoma*. PLoS Med, 2008. **5**(1): p. e8.
142. Rodriguez, C.I., et al., *High-efficiency deleter mice show that FLPe is an alternative to Cre-loxP*. Nat Genet, 2000. **25**(2): p. 139-40.
143. Schwander, M., et al., *Beta1 integrins regulate myoblast fusion and sarcomere assembly*. Dev Cell, 2003. **4**(5): p. 673-85.
144. Polak, P., et al., *Adipose-specific knockout of raptor results in lean mice with enhanced mitochondrial respiration*. Cell Metab, 2008. **8**(5): p. 399-410.
145. Popovic, Z.B., et al., *Differences in left ventricular long-axis function from mice to humans follow allometric scaling to ventricular size*. J Physiol, 2005. **568**(Pt 1): p. 255-65.
146. Laws, N. and A. Hoey, *Progression of kyphosis in mdx mice*. J Appl Physiol, 2004. **97**(5): p. 1970-7.
147. Ringelmann, B., et al., *Expression of laminin alpha1, alpha2, alpha4, and alpha5 chains, fibronectin, and tenascin-C in skeletal muscle of dystrophic 129ReJ dy/dy mice*. Exp Cell Res, 1999. **246**(1): p. 165-82.
148. Austyn, J.M. and S. Gordon, *F4/80, a monoclonal antibody directed specifically against the mouse macrophage*. Eur J Immunol, 1981. **11**(10): p. 805-15.
149. Sorokin, L.M., et al., *Developmental regulation of the laminin alpha5 chain suggests a role in epithelial and endothelial cell maturation*. Dev Biol, 1997. **189**(2): p. 285-300.
150. Sewry, C.A., et al., *The spectrum of pathology in central core disease*. Neuromuscul Disord, 2002. **12**(10): p. 930-8.
151. Sandri, M., et al., *Foxo transcription factors induce the atrophy-related ubiquitin ligase atrogin-1 and cause skeletal muscle atrophy*. Cell, 2004. **117**(3): p. 399-412.
152. Stitt, T.N., et al., *The IGF-1/PI3K/Akt pathway prevents expression of muscle atrophy-induced ubiquitin ligases by inhibiting FOXO transcription factors*. Mol Cell, 2004. **14**(3): p. 395-403.
153. Sakamoto, K. and L.J. Goodyear, *Invited review: intracellular signaling in contracting skeletal muscle*. J Appl Physiol, 2002. **93**(1): p. 369-83.
154. Kumar, A., et al., *Muscle-specific deletion of rictor impairs insulin-stimulated glucose transport and enhances Basal glycogen synthase activity*. Mol Cell Biol, 2008. **28**(1): p. 61-70.
155. Treves, S., et al., *Congenital muscle disorders with cores: the ryanodine receptor calcium channel paradigm*. Curr Opin Pharmacol, 2008.
156. Handschin, C., et al., *Abnormal glucose homeostasis in skeletal muscle-specific PGC-1alpha knockout mice reveals skeletal muscle-pancreatic beta cell crosstalk*. The Journal of clinical investigation, 2007. **117**(11): p. 3463-74.
157. Winkel, L.P., et al., *The natural course of non-classic Pompe's disease; a review of 225 published cases*. J Neurol, 2005. **252**(8): p. 875-84.
158. Song, X.M., et al., *Muscle fiber type specificity in insulin signal transduction*. The American journal of physiology, 1999. **277**(6 Pt 2): p. R1690-6.
159. Wende, A.R., et al., *A Role for the Transcriptional Coactivator PGC-1{alpha} in Muscle Refueling*. J Biol Chem, 2007. **282**(50): p. 36642-51.
160. Leone, T.C., et al., *PGC-1alpha deficiency causes multi-system energy metabolic derangements: muscle dysfunction, abnormal weight control and hepatic steatosis*. PLoS Biol, 2005. **3**(4): p. e101.
161. Handschin, C., et al., *Skeletal muscle fiber-type switching, exercise intolerance, and myopathy in PGC-1alpha muscle-specific knock-out animals*. J Biol Chem, 2007. **282**(41): p. 30014-21.
162. Bassel-Duby, R. and E.N. Olson, *Signaling pathways in skeletal muscle remodeling*. Annual review of biochemistry, 2006. **75**: p. 19-37.

163. Potthoff, M.J., et al., *Histone deacetylase degradation and MEF2 activation promote the formation of slow-twitch myofibers*. J Clin Invest, 2007. **117**(9): p. 2459-67.
164. Wu, H., et al., *MEF2 responds to multiple calcium-regulated signals in the control of skeletal muscle fiber type*. Embo J, 2000. **19**(9): p. 1963-73.
165. Gollnick, P.D., et al., *Elongation of skeletal muscle relaxation during exercise is linked to reduced calcium uptake by the sarcoplasmic reticulum in man*. Acta Physiol Scand, 1991. **142**(1): p. 135-6.
166. Wiedmann, M., et al., *PI3K/Akt-dependent regulation of the transcription factor myocyte enhancer factor-2 in insulin-like growth factor-1- and membrane depolarization-mediated survival of cerebellar granule neurons*. Journal of neuroscience research, 2005. **81**(2): p. 226-34.
167. Manning, B.D., *Balancing Akt with S6K: implications for both metabolic diseases and tumorigenesis*. The Journal of cell biology, 2004. **167**(3): p. 399-403.
168. Beals, C.R., et al., *Nuclear export of NF-ATc enhanced by glycogen synthase kinase-3*. Science, 1997. **275**(5308): p. 1930-4.
169. Wu, H., et al., *NFAT signaling and the invention of vertebrates*. Trends Cell Biol, 2007. **17**(6): p. 251-60.
170. Alessi, D.R., et al., *Characterization of a 3-phosphoinositide-dependent protein kinase which phosphorylates and activates protein kinase Balpha*. Curr Biol, 1997. **7**(4): p. 261-9.
171. Bayascas, J.R. and D.R. Alessi, *Regulation of Akt/PKB Ser473 phosphorylation*. Mol Cell, 2005. **18**(2): p. 143-5.
172. Dunant, P., et al., *Expression of dystrophin driven by the 1.35-kb MCK promoter ameliorates muscular dystrophy in fast, but not in slow muscles of transgenic mdx mice*. Mol Ther, 2003. **8**(1): p. 80-9.
173. Osoegawa, K., et al., *Bacterial artificial chromosome libraries for mouse sequencing and functional analysis*. Genome Res, 2000. **10**(1): p. 116-28.
174. Casanova, E., et al., *Construction of a conditional allele of RSK-B/MSK2 in the mouse*. Genesis, 2002. **32**(2): p. 158-60.
175. Nagy, A., et al., *Derivation of completely cell culture-derived mice from early-passage embryonic stem cells*. Proc Natl Acad Sci U S A, 1993. **90**(18): p. 8424-8.
176. Graus-Porta, D., et al., *Beta1-class integrins regulate the development of laminae and folia in the cerebral and cerebellar cortex*. Neuron, 2001. **31**(3): p. 367-79.
177. Delbono, O., et al., *Loss of skeletal muscle strength by ablation of the sarcoplasmic reticulum protein JP45*. Proc Natl Acad Sci U S A, 2007. **104**(50): p. 20108-13.
178. Brussee, V., F. Tardif, and J.P. Tremblay, *Muscle fibers of mdx mice are more vulnerable to exercise than those of normal mice*. Neuromuscul Disord, 1997. **7**(8): p. 487-92.
179. Moll, J., et al., *An agrin minigene rescues dystrophic symptoms in a mouse model for congenital muscular dystrophy*. Nature, 2001. **413**(6853): p. 302-7.
180. Briguët, A., et al., *Histological parameters for the quantitative assessment of muscular dystrophy in the mdx-mouse*. Neuromuscul Disord, 2004. **14**(10): p. 675-82.

11. CURRICULUM VITAE

CONTACT INFORMATION

Name: Bentzinger Conrad Florian
Address: Division Pharmacology / Neurobiology
Biozentrum, University of Basel
Klingelbergstr. 50/70
CH-4056 Basel / Switzerland
Email: Cf.Bentzinger@unibas.ch

PERSONAL INFORMATION

Date of Birth: 24.01.1977
Place of Birth: Basel
Citizenship: Swiss
Sex: male

PROFESSIONAL EXPERIENCE

Feb. 2006 – Feb. 2009 Ph.D. thesis in the group of Prof. Markus A. Ruegg, Biozentrum, University of Basel, Title: "Function of mTOR complex 1 and 2 in Skeletal Muscle"
Dec. 2004 - Feb. 2006 Civilian national service (ProNatura AG / Biozentrum, University of Basel)
2003 - 2004 Diploma thesis at the Biozentrum, University of Basel, Title: "Overexpression of mini-agrin in skeletal muscle increases muscle integrity and regenerative capacity in laminin-alpha2-deficient mice"
2002 - 2003 Internships in Neurobiology, Cellbiology, Biochemistry, Immunology, Biophysics and Microbiology during studies
2002 Internship in pharmaceutical biology at Vitaplant AG
1998 Internship at Ciba Spezialitätenchemie

EDUCATION

University: 2000 - 2004 Studies of molecular biology at the University of Basel
Degree: Diploma in Biology
High School: 1998 - 2000 Gymnasialstufe Minerva-Schulen Basel
Degree: Eidgenössische Maturität, Typ E
1994 - 1998 Diplomabteilung Kantonale Handelsschule Basel
Degree: Kantonales Handelsdiplom
1989 - 1993 Mathematisch naturwissenschaftliches Gymnasium, Basel

LANGUAGES

German (mother tongue)
English (fluent)
French (intermediate level)

PUBLICATIONS

Bentzinger, C.F., Romanino, K., Cloëtta, D., Lin, S., Mascarenhas, J.B., Oliveri, F., Xia, J., Casanova, E., Costa, C.F., Brink, M., Zorzato, F., Hall, M.N., Ruegg, M.A. (2008). Skeletal muscle-specific ablation of raptor, but not of rictor, causes metabolic changes and results in muscle dystrophy. *Cell Metabolism*, Volume 8, Issue 5, 5 November 2008, Pages 411-424

Bentzinger, C.F., Barzaghi, P., Lin, S., and Ruegg, M.A. (2005). Overexpression of mini-agrin in skeletal muscle increases muscle integrity and regenerative capacity in laminin- α 2 deficient mice. *FASEB JOURNAL*, Volume 19, Issue 8, June 2005, Pages: 934-942

Bezakova, G., Bentzinger, C.F., Maj, G., Brenner, H.R., Stebler, M., Ruegg, M.A. Gene profiling at the NMJ revealing novel roles for mapkinase signalling (in preparation)

Galic, M., Kriz, A., Vigot, R., Zhang, Y.P., Bezakova, G., Bentzinger, C.F., Stebler, M., Bettler, B., Oertner, T.G., Ruegg, M.A. Regulation of dendritic spine morphogenesis and synapse formation by Copines (in preparation)

FELLOWSHIPS

Fellowship of the Roche Research Foundation for two years of Ph.D. work.

NETWORKS

Partner involved in the TREAT-NMD neuromuscular network of excellence

12. ACKNOWLEDGEMENTS

First and foremost, I would like to express my deepest sense of gratitude to Prof. Markus Rüegg for being a dedicated, sympathetic, inspiring and supportive mentor.

My sincere thanks also go to Gabriela Bezakova and Shuo Lin who were always around for fruitful discussions and from whom I learned about many experimental techniques.

Furthermore I would like to thank all the people involved in my project, especially Klaas Romanino, Shuo Lin, Dimitri Cloëtta, Filippo Oliveri, Francesco Zozato and Michael Hall.

Professors Michael Hall and Francesco Zorzato also deserve special thanks for being thesis committee members.

I gratefully acknowledge the support from the Roche Research Foundation given to this project.

Furthermore, I feel very grateful to all the members of the Ruegg group for the great atmosphere and collegueship in and out of the lab.

My sincere love goes to Andrea for her friendship and support and for bringing a lot of sunshine into my life.

Last but not least, I am deeply and forever indebted to my parents for their love and indispensable support.